# Group 4 permethylindenyl constrained geometry complexes for ethylene polymerisation catalysis

Thomas J. Williams, Jean-Charles Buffet, Zoë R. Turner, and Dermot O'Hare

Chemistry Research Laboratory, Department of Chemistry, University of Oxford, 12 Mansfield Road, OX1 3TA, Oxford, UK.

## Table of Contents

# 1 Experimental techniques and physical methods

**General procedures.** Air and moisture sensitive techniques were undertaken in an inert atmosphere of nitrogen, using standard Schlenk techniques,[1] on a dual manifold nitrogen/vacuum line or in an MBraun Unilab glovebox. Pentane, hexane, toluene, benzene, were dried using an MBraun SPS 800 solvent purification system. Tetrahydrofuran (THF) and diethyl ether were distilled from purple Na/benzophenone indicator. Amines (*tert*-butylamine, *iso*-propylamine, 4-*tert*-butylaniline, 4-*n*-butylaniline, aniline, *n*-butylamine and 2,6-diisopropylaniline) were freeze-pump-thaw degassed 3 times. The amines and THF were stored over pre-activated 3 Å molecular sieves; hexane, benzene and toluene were stored on a potassium mirror. Deuterated solvents were dried over K ($C_6D_6$) or $CaH_2$ ($C_5D_5N$), freeze-pump-thaw degassed, vacuum transferred and stored over pre-activated 3 Å molecular sieves. Ind*$SiMe_2Cl$ was synthesised using a literature procedure from hexamethylindene ($Ind^{\#}H$).[2] Lithium amides were prepared via lithiation of an amine with 1.1 equivalents of *n*-BuLi. $TiCl_4 \cdot 2THF$ was synthesised *via* a literature procedure from $TiCl_4$.[3]

**Solution phase NMR spectroscopy.** NMR spectra were recorded on either a 400 MHz Bruker Avance III HD nanobay spectrometer or a 500 MHz Bruker Avance III HD nanobay spectrometer. $^1H$ and $^{13}C\{^1H\}$ spectra were recorded at 298 K unless otherwise stated, referenced internally to the residual protio-solvent peak in the deuterated solvent. Air-sensitive samples were prepared in a glovebox under an inert atmosphere, using dried deuterated solvents in Young's NMR tubes.

**Solid-state NMR spectroscopy.** All experiments were carried out by Dr. Nicholas Rees (University of Oxford). Compounds were prepared in a glovebox under a nitrogen atmosphere and sealed in 5 mm Young's type NMR tubes. Spectra were recorded on a Bruker Avance III HD NanoBay 400.2 MHz Solid-state NMR spectrometer, samples were spun at the magic angle (54.71°) at spin rates 10 kHz for $^{13}C$ CP-MAS, $^{27}Al$ DP-MAS, and $^{29}Si$ CP-MAS. $^{13}C$ NMR spectra were referenced to adamantane, $^{27}Al$ to $Al(NO_3)_3$.

**X-ray crystallography.** Crystals were mounted on MiTeGen MicroMounts using perfluoropolyether oil and rapidly transferred to a goniometer head on a diffractometer fitted with and Oxford Cryosystems Cryostream open-flow nitrogen-cooling device.[4] Data collections were carried out at 150 K on an Oxford Diffraction Supernova Diffractometer using mirror-monochromated Cu *Kα* radiation (λ= 1.54178 Å) and data was processed using CrysAlisPro.[5] The structures were solved using direct methods (SIR-92)[6] or using a charge-flipping procedure (SuperFlip)[7] and refined by full-matrix least squares using the WinGX programme suite.[8] Interplanar distances and angles were calculated using PLATON.[9] Molecular structures were generated using ORTEP3.[10] Percentage buried volume was calculated using SambVca.[11]

**Elemental analysis.** Samples were prepared in a glovebox and measured by Mr Stephen Boyer (London Metropolitan University).

**Scanning electron microscopy.** Scanning electron microscopy (SEM) images were collected by Mr Phakpoom Angpanitcharoen and Miss Jessica Lamb (University of Oxford), on a JEOL JSM 6610 scanning electron microscope. Particles were cast onto a silica wafer. Before imaging, the samples were coated with platinum to prevent charging, improving the image quality. Energy dispersive X-ray (EDX) spectroscopy was also performed on this instrument to determine the relative percentages of elements on the surface.

**Inductively Coupled Plasma optical emission spectrometry (ICP-OES).** ICP-OES data were collected on a Agilent 5110 ICP-OES with VistaChip II CCD detector at HTExplore (University of Naples).

**Differential Scanning Calorimetry (DSC).** Samples were run on a DSC3+ (Mettler Toledo, Ltd) using 5 mg of polyethylene in a sealed aluminium 100 µL crucible. An empty crucible was used as a reference, and the DSC was calibrated using indium. Samples were heated from 25 to 250 °C and cooled back again at a rate of 5 °C per minute, a total of three cycles were run. Polymer melt temperature values were taken from the third heating cycle.

# 2 NMR spectroscopy

## 2.1 Solution NMR spectroscopy

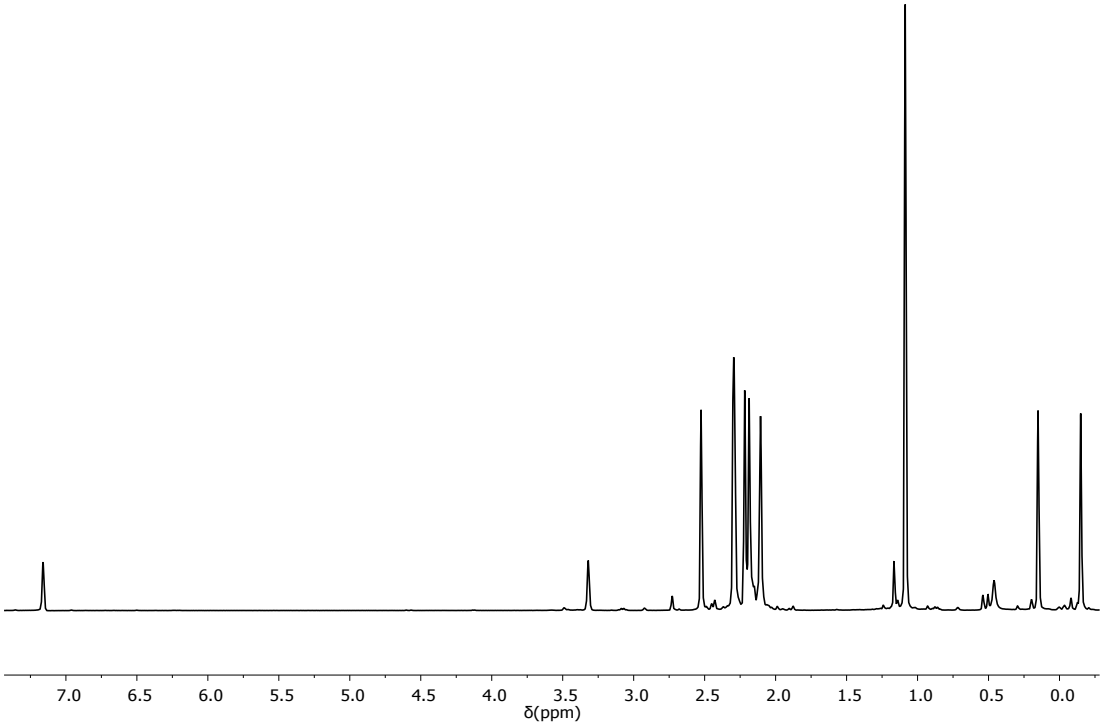


**Fig. S1** $^{1}$H NMR spectrum of $^{Me2}$SB($^{t\text{-Bu}}$N,I*)$H_2$ (400.2 MHz, $C_6D_6$, 298 K).

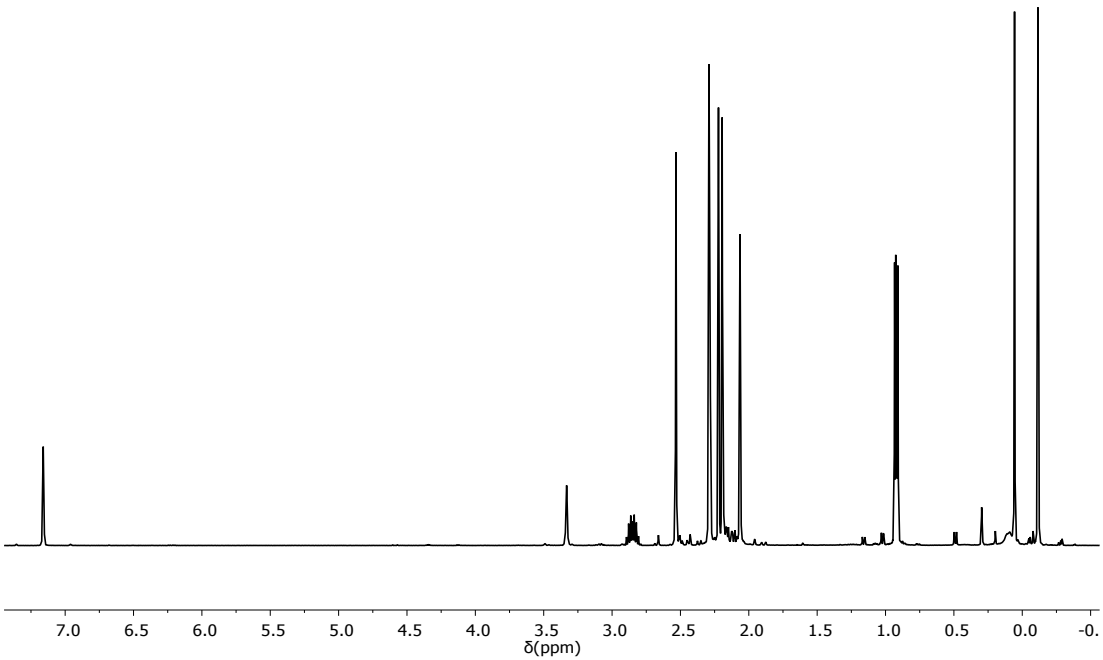


**Fig. S2** $^{1}$H NMR spectrum of $^{Me2}$SB($^{i\text{-Pr}}$N,I*)$H_2$ (400.2 MHz, $C_6D_6$, 298 K).

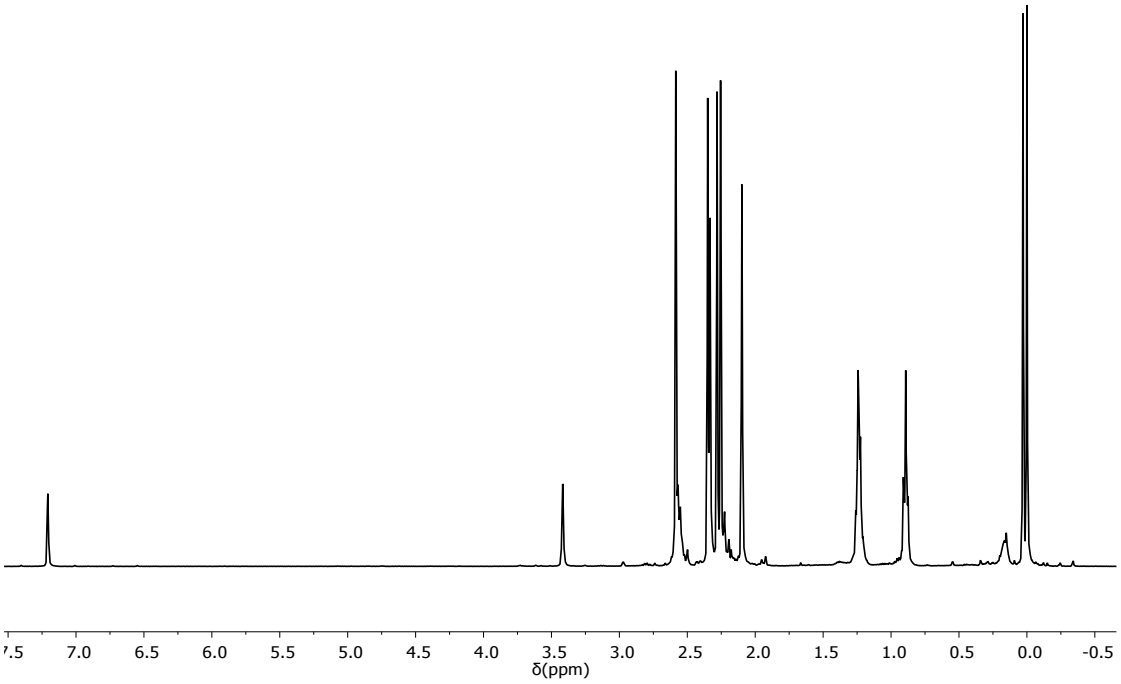


**Fig. S3** $^{1}$H NMR spectrum of $^{Me2}$SB($^{n\text{-}Bu}$N,I*)$H_2$ (499.9 MHz, $C_6D_6$, 298 K).

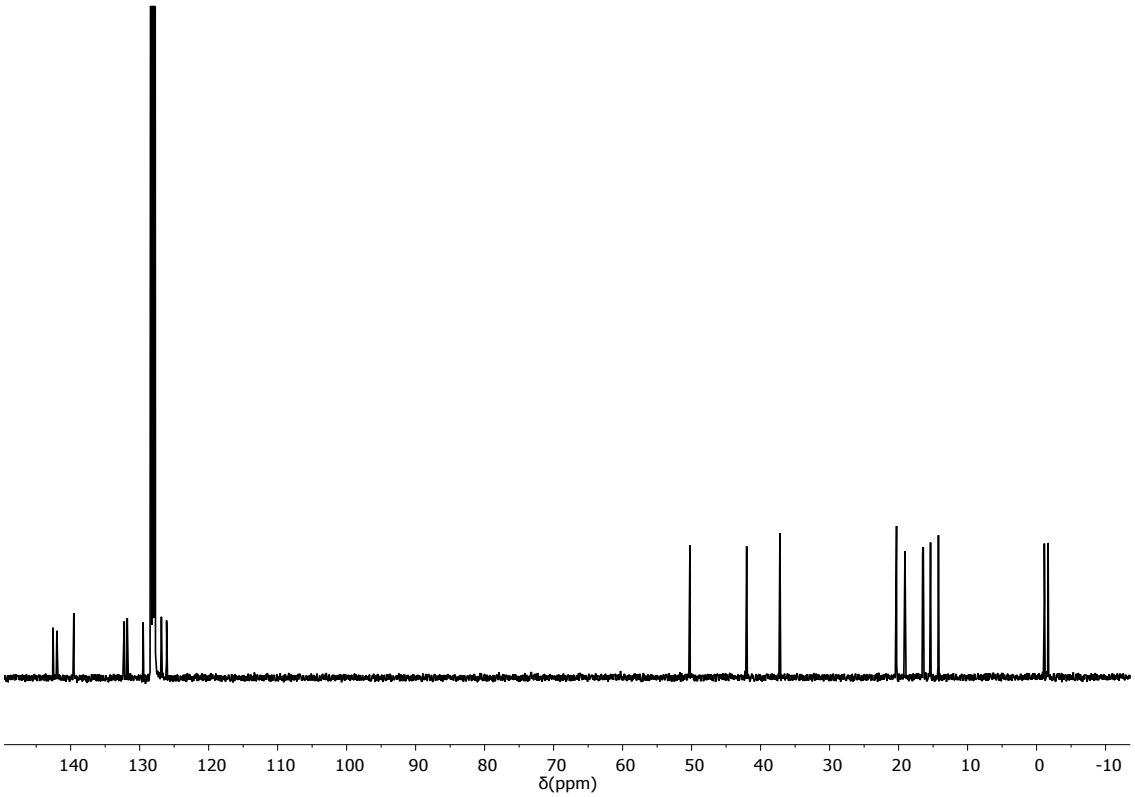


**Fig. S4** $^{13}$C{$^{1}$H} NMR spectrum of $^{Me2}$SB($^{n\text{-}Bu}$N,I*)$H_2$ (125.7 MHz, $C_6D_6$, 298 K).

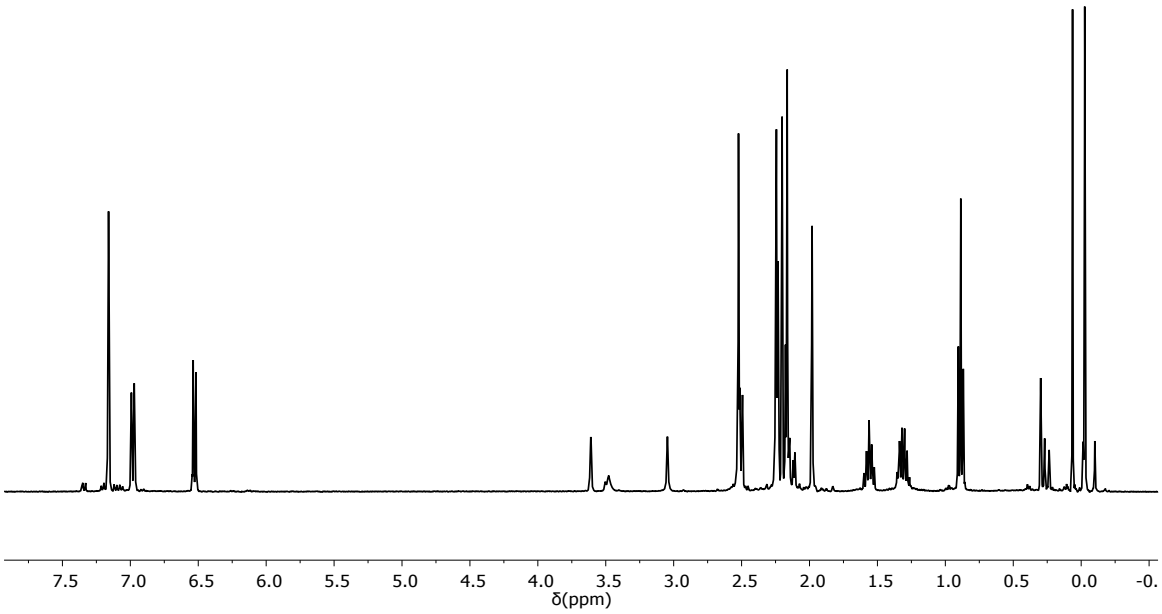


**Fig. S5** $^{1}$H NMR spectrum of $^{Me2}$SB($^{4\text{-}n\text{-Bu-C}_6H_4}$N,I*)$H_2$ (400.2 MHz, $C_6D_6$, 298 K).

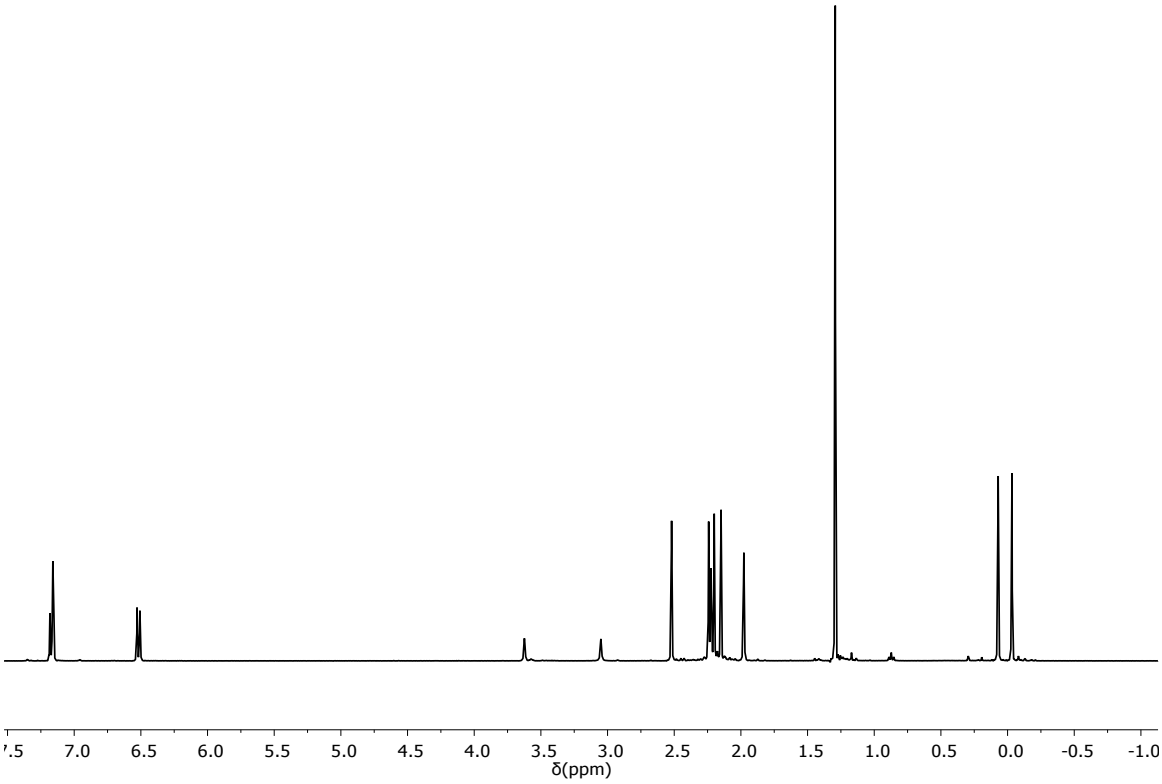


**Fig. S6** $^{1}$H NMR spectrum of $^{Me2}$SB($^{4\text{-}n\text{-Bu-C}_6H_4}$N,I*)$H_2$ (400.2 MHz, $C_6D_6$, 298 K).

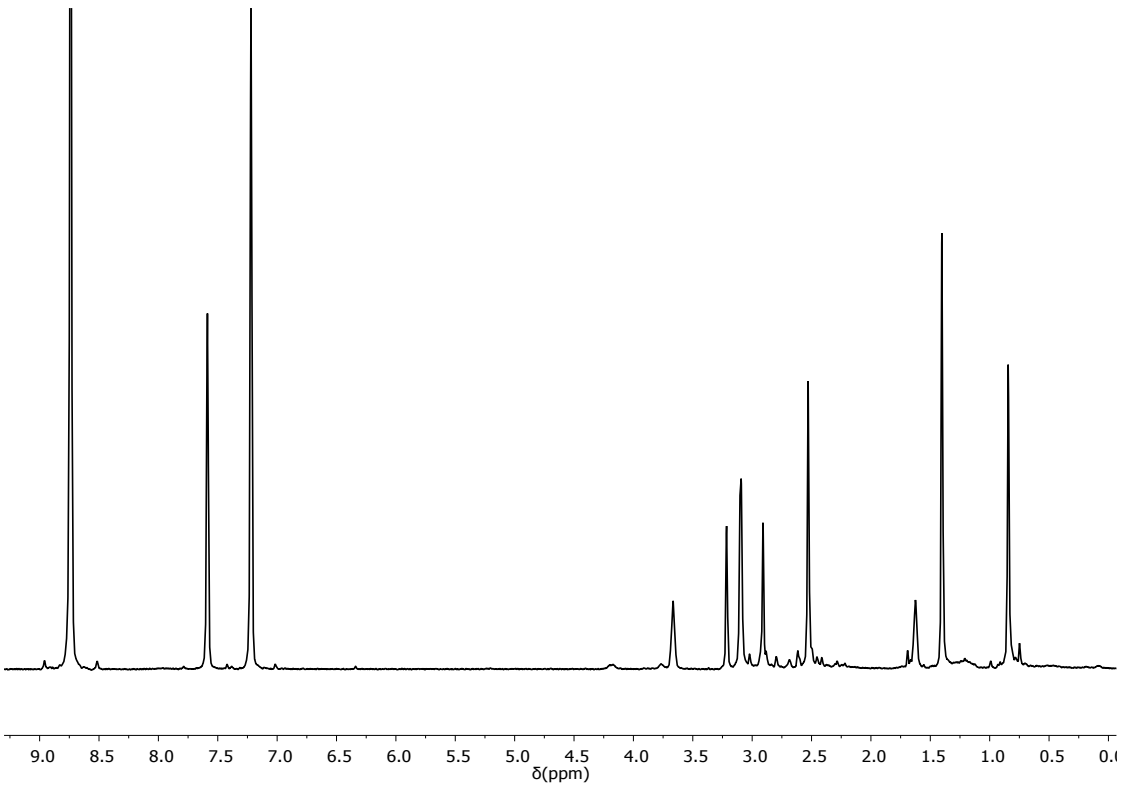


**Fig. S7** $^{1}$H NMR spectrum of $^{Me2}$SB($^{t\text{-Bu}}$N,I*)$Li_2$ (400.2 MHz, $C_5D_5N$, 298 K).

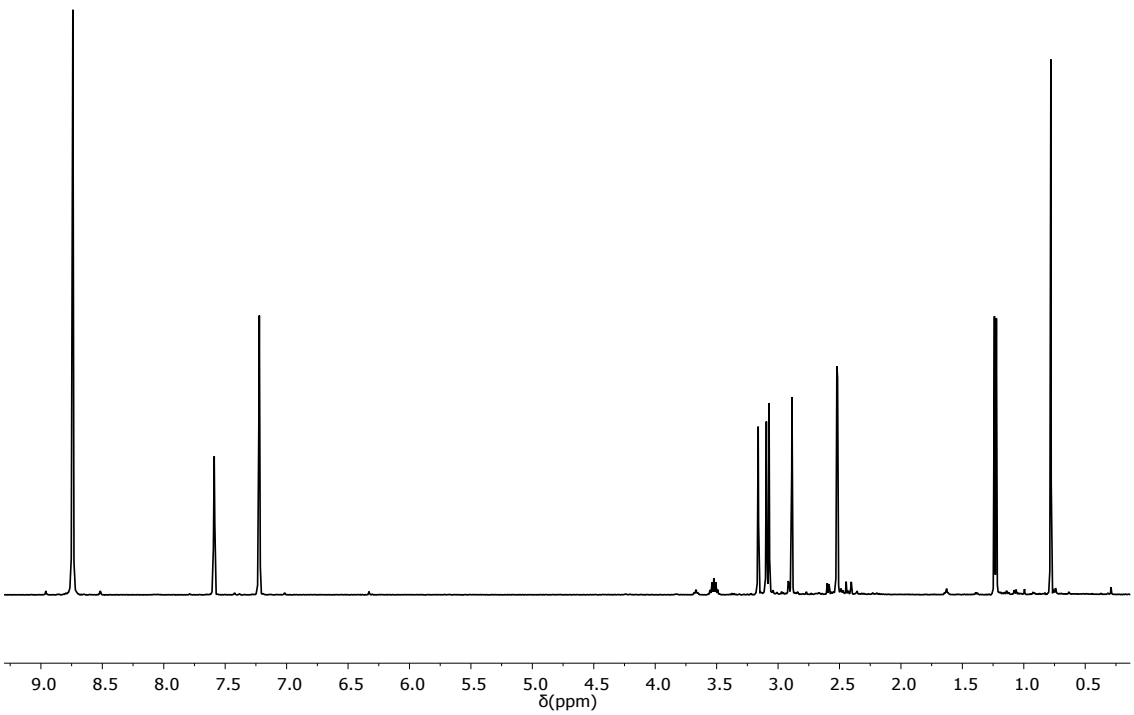


**Fig. S8** $^{1}$H NMR spectrum of $^{Me2}$SB($^{i\text{-Pr}}$N,I*)$Li_2$ (400.2 MHz, $C_5D_5N$, 298 K).

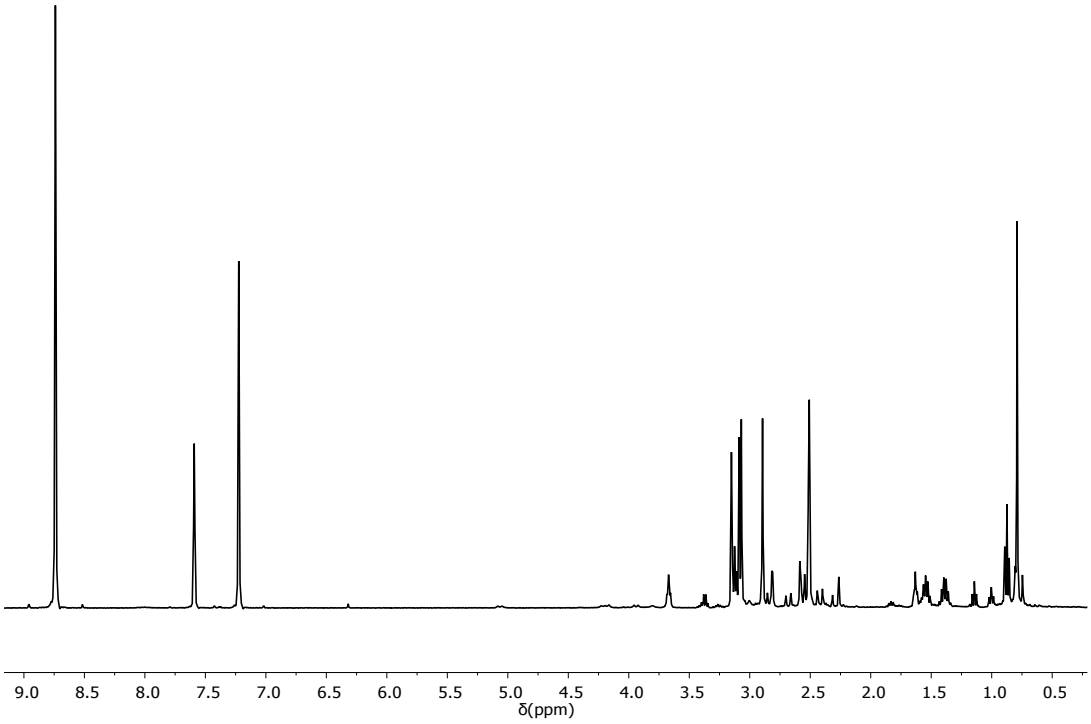


**Fig. S9** $^{1}$H NMR spectrum of $^{Me2}$SB($^{n\text{-}Bu}$N,I*)$Li_2$ (400.2 MHz, $C_5D_5N$, 298 K).

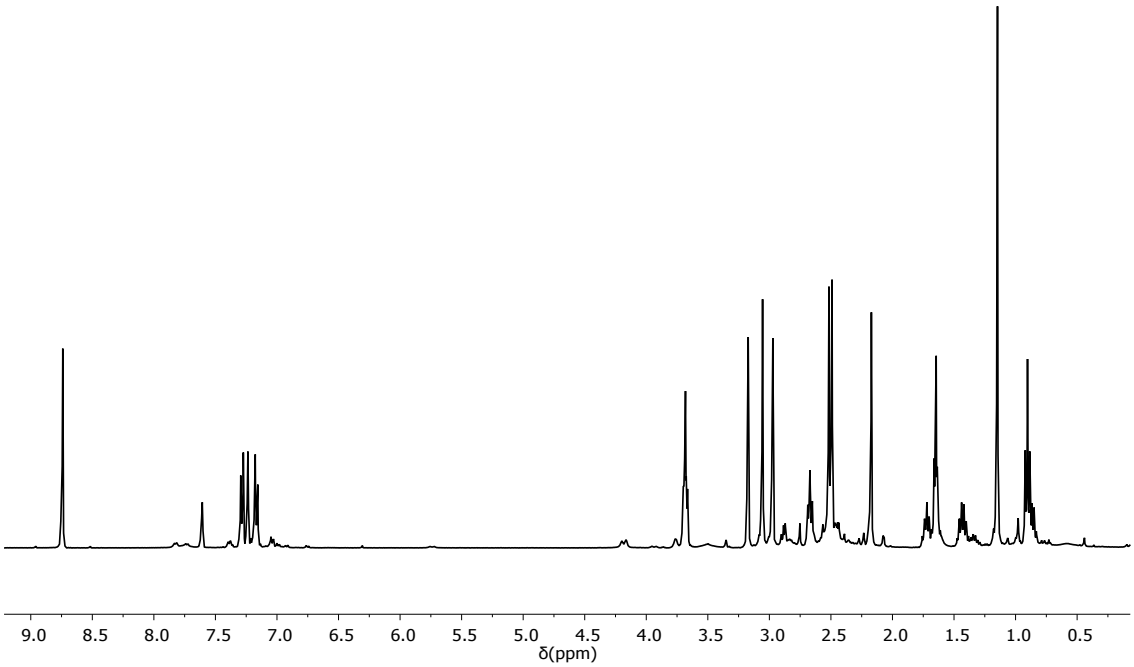


**Fig. S10** $^{1}$H NMR spectrum of $^{Me2}$SB($^{4\text{-}n\text{-}Bu\text{-}C_6H_4}$N,I*)$Li_2$ (400.2 MHz, $C_5D_5N$, 298 K).

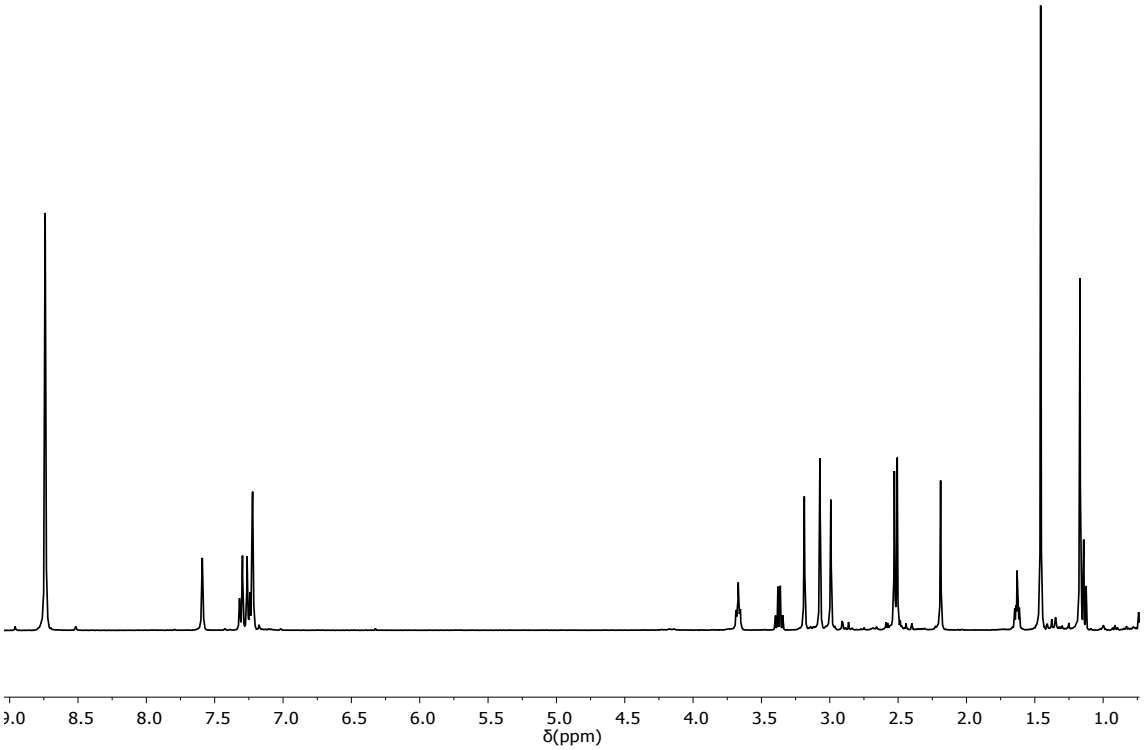


**Fig. S11** $^{1}$H NMR spectrum of $^{Me2}$SB($^{4\text{-}t\text{-}Bu\text{-}C_6H_4}$N,I*)$Li_2$ (400.2 MHz, $C_5D_5N$, 298 K).

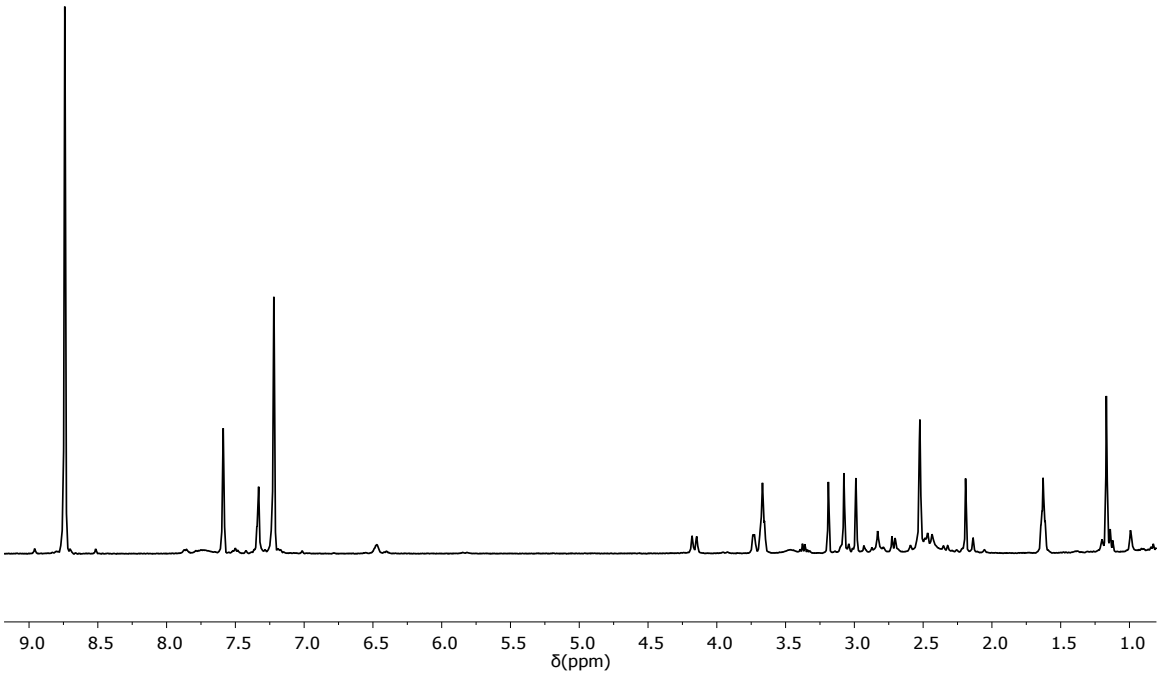


**Fig. S12** $^{1}$H NMR spectrum of $^{Me2}$SB($^{Ph}$N,I*)$Li_2$ (400.2 MHz, $C_5D_5N$, 298 K).

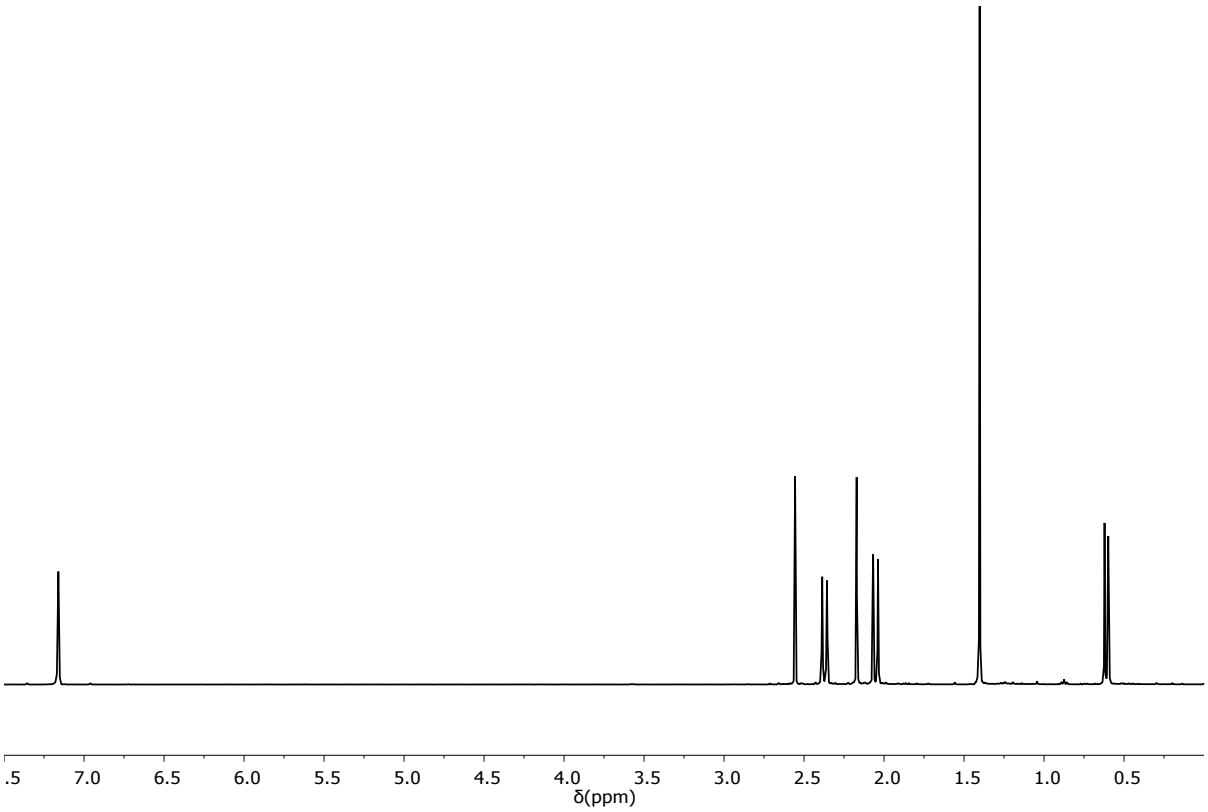


**Fig. S13** $^{1}$H NMR spectrum of $^{Me2}$SB($^{t\text{-}Bu}$N,I*)TiCl$_2$ (400.2 MHz, $C_6D_6$, 298 K).

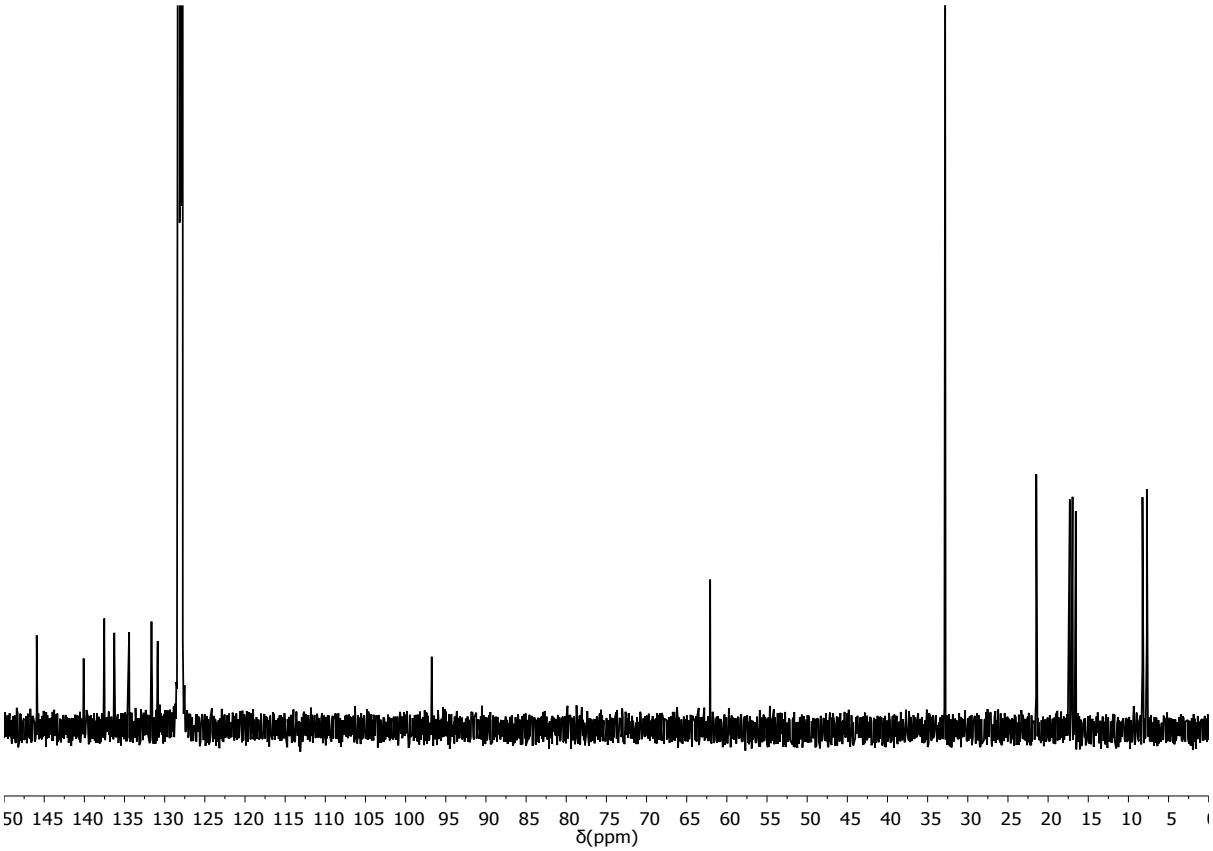


**Fig. S14** $^{13}$C{$^{1}$H} NMR spectrum of $^{Me2}$SB($^{t\text{-}Bu}$N,I*)TiCl$_2$ (125.7 MHz, $C_6D_6$, 298 K).

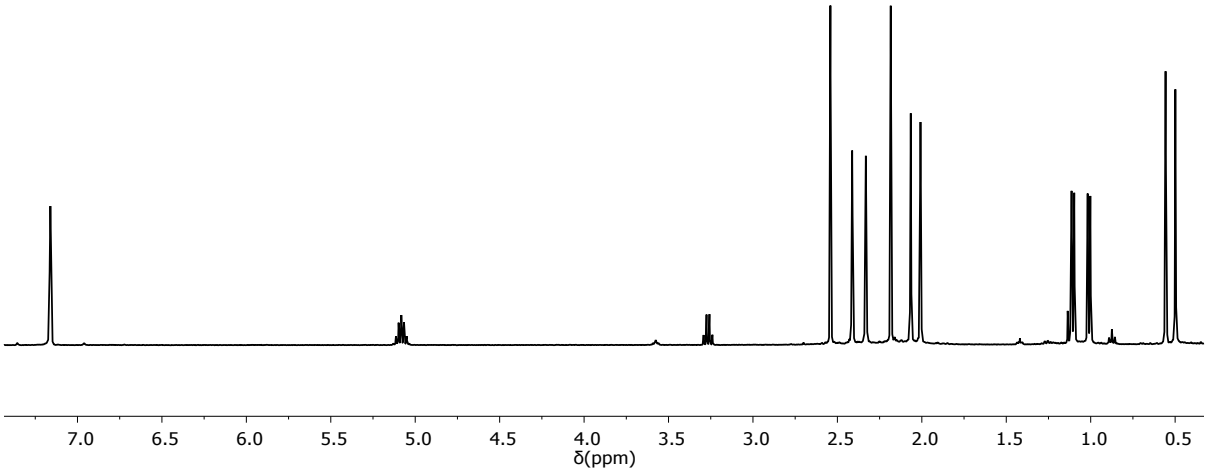


**Fig. S15** $^{1}$H NMR spectrum of $^{Me2}$SB($^{i\text{-}Pr}$N,I*)TiCl$_2$ (400.2 MHz, $C_6D_6$, 298 K).

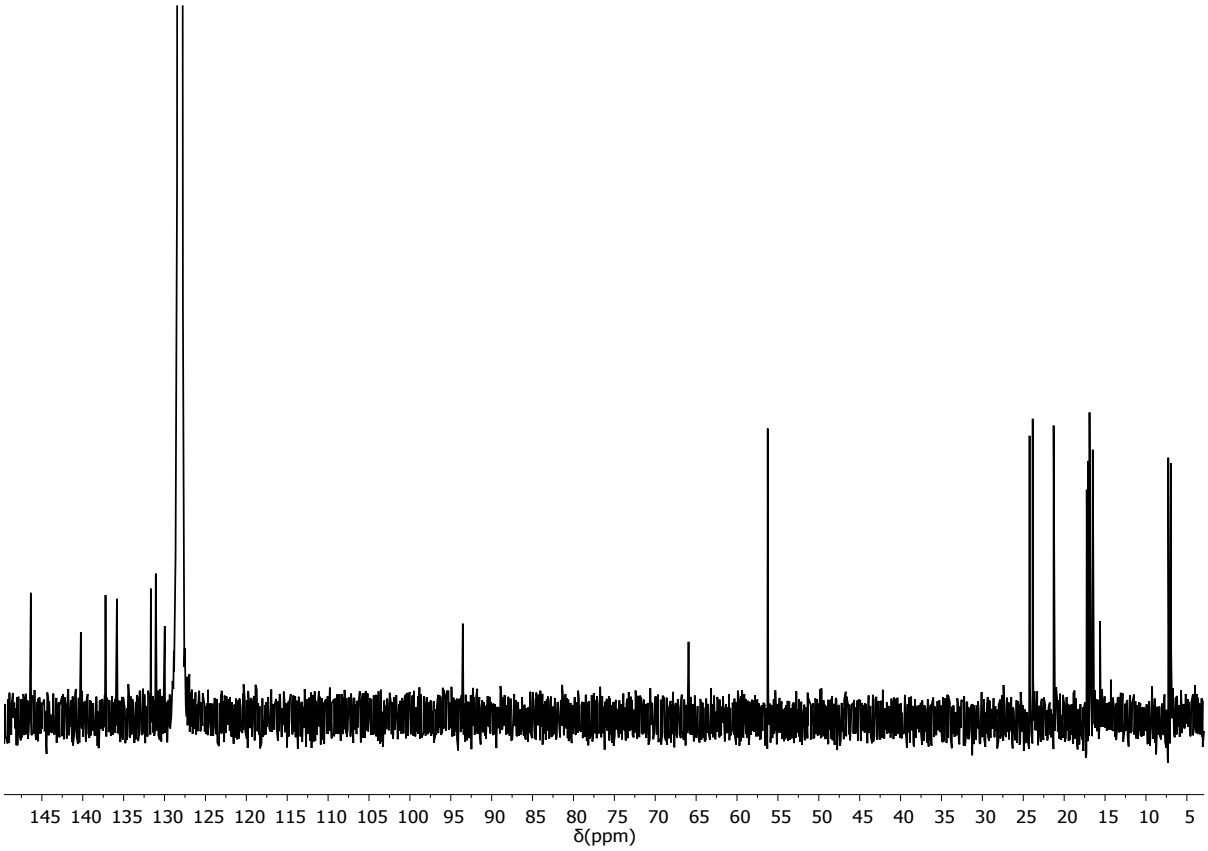


**Fig. S16** $^{13}$C{$^{1}$H} NMR spectrum of $^{Me2}$SB($^{i\text{-}Pr}$N,I*)TiCl$_2$ (125.7 MHz, $C_6D_6$, 298 K).

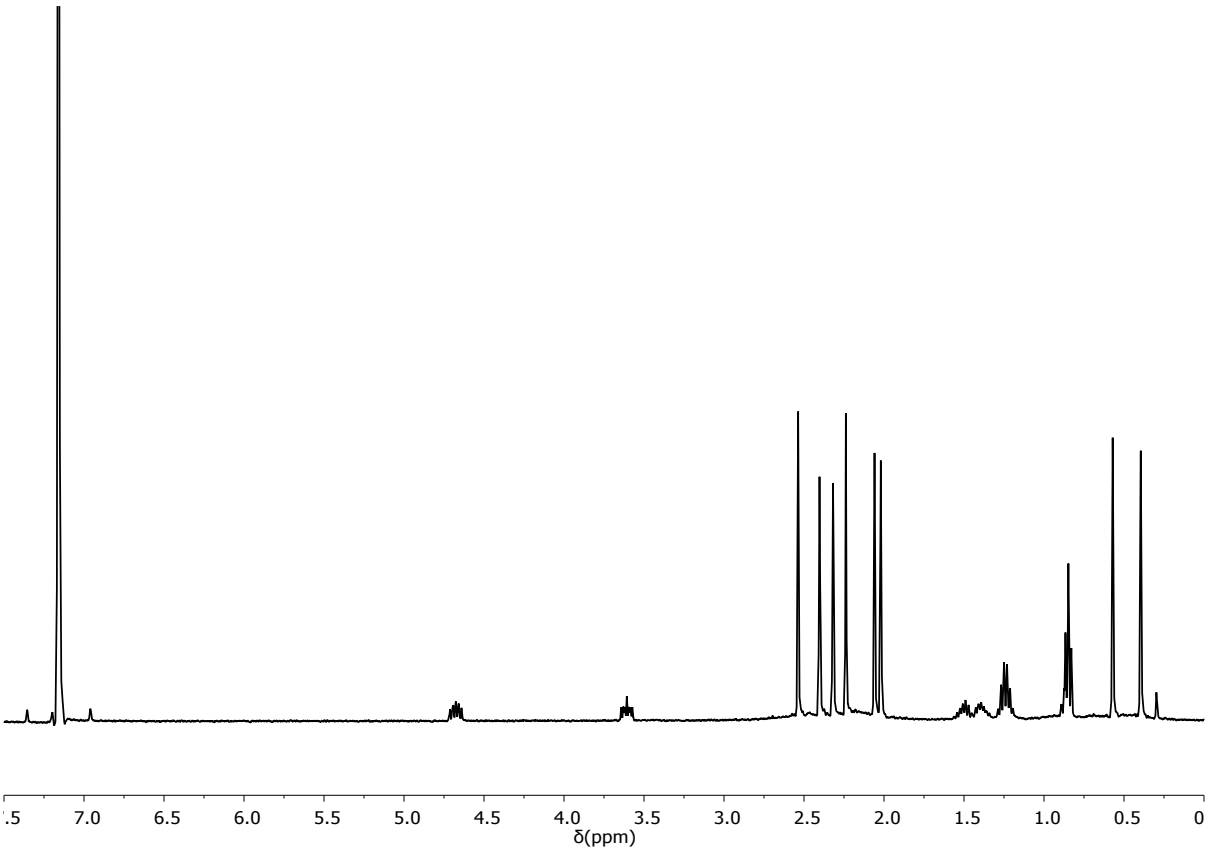


**Fig. S17** $^{1}$H NMR spectrum of $^{Me2}$SB($^{n\text{-Bu}}$N,I*)TiCl$_2$ (400.2 MHz, $C_6D_6$, 298 K).

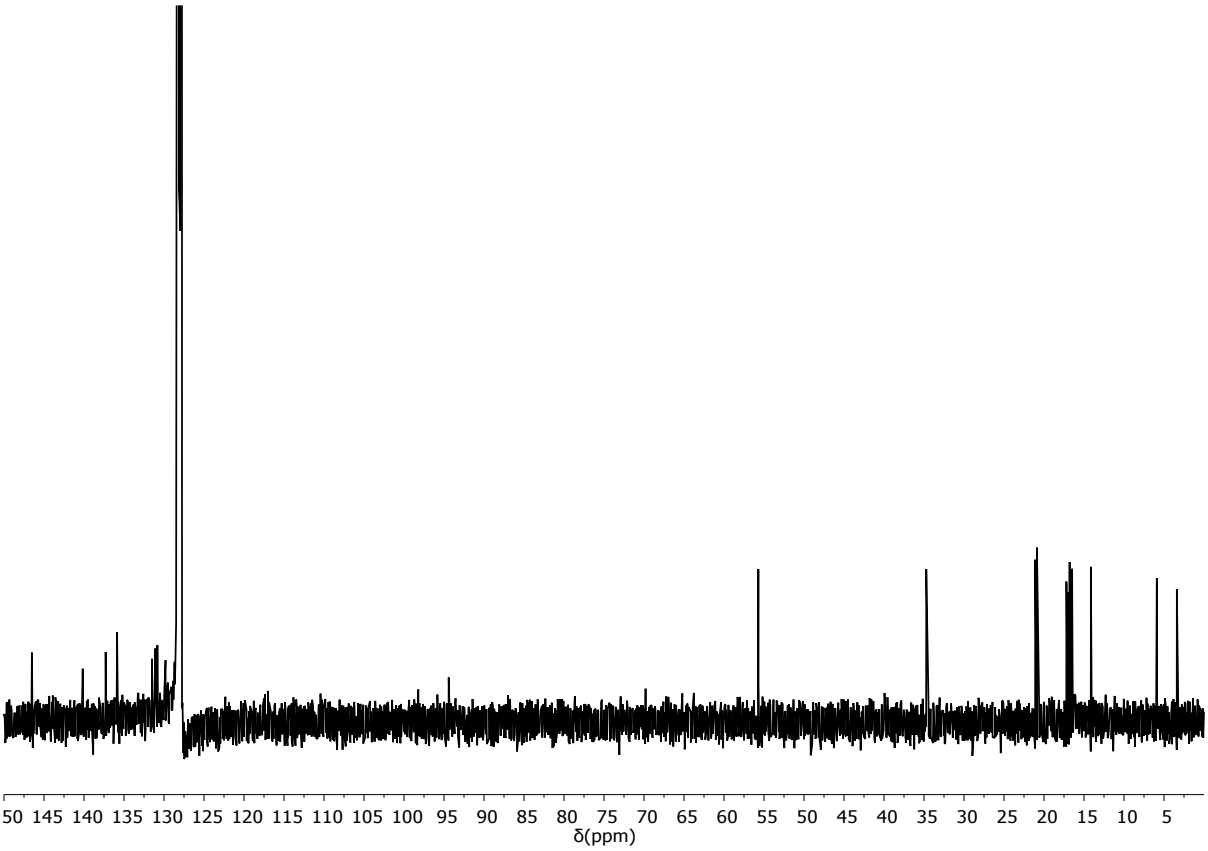


**Fig. S18** $^{13}$C{$^{1}$H} NMR spectrum of $^{Me2}$SB($^{n\text{-Bu}}$N,I*)TiCl$_2$ (125.7 MHz, $C_6D_6$, 298 K).

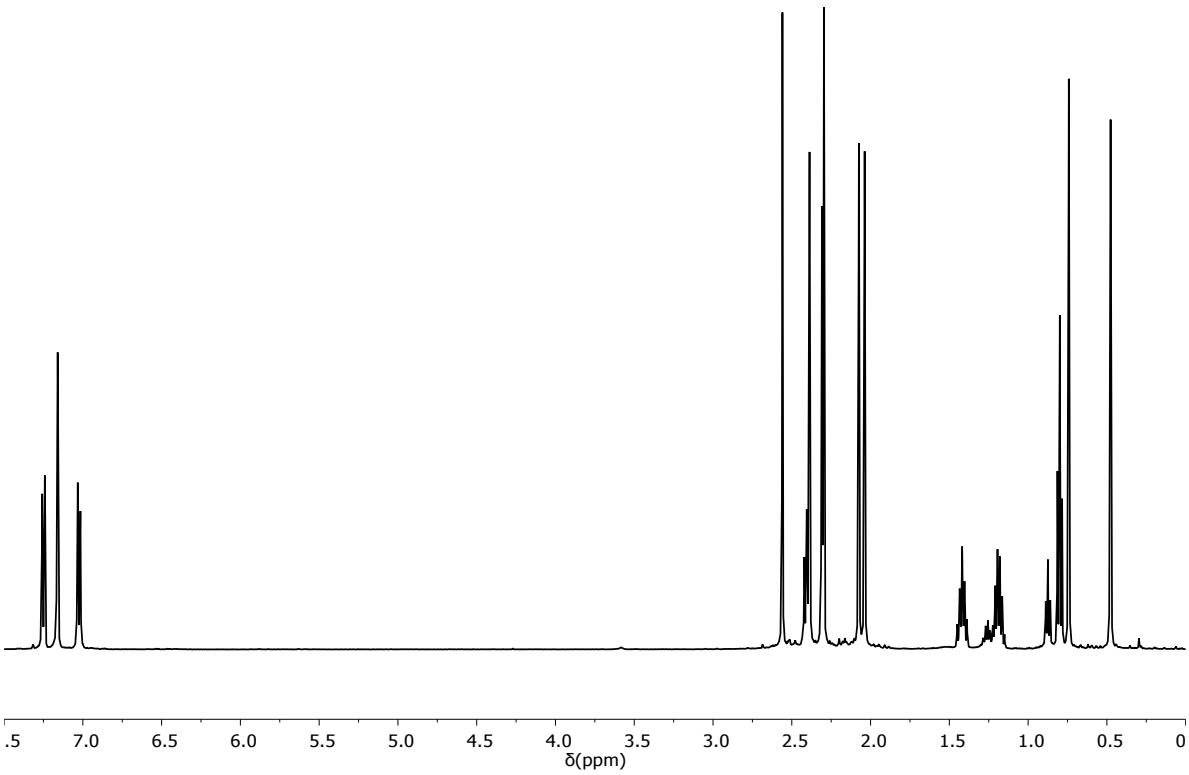


**Fig. S19** $^{1}$H NMR spectrum of $^{Me2}$SB($^{4\text{-}n\text{-Bu-C6H4}}$N,I*)TiCl$_2$, (pentane: 0.87 and 1.23 ppm; 499.9 MHz, $C_6D_6$, 298 K).

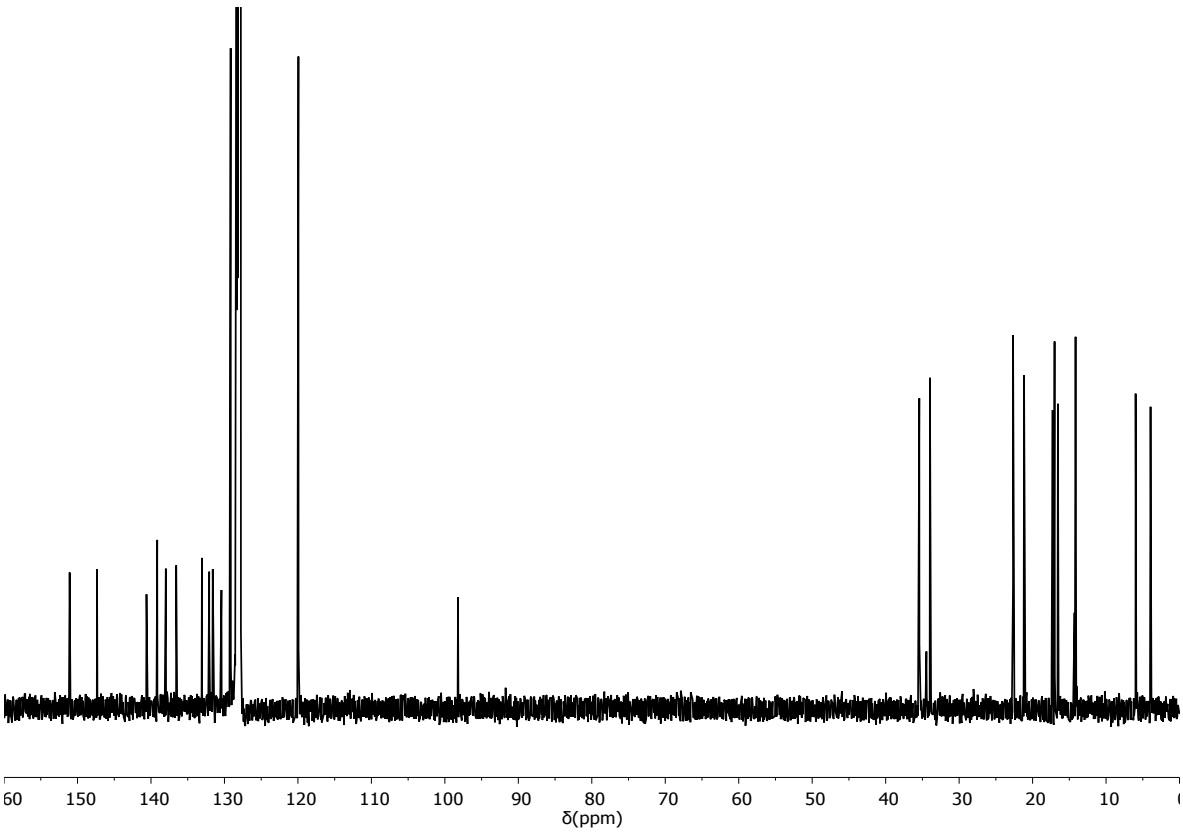


**Fig. S20** $^{13}$C{$^{1}$H} NMR spectrum of $^{Me2}$SB($^{4\text{-}n\text{-Bu-C6H4}}$N,I*)TiCl$_2$ (125.7 MHz, $C_6D_6$, 298 K).

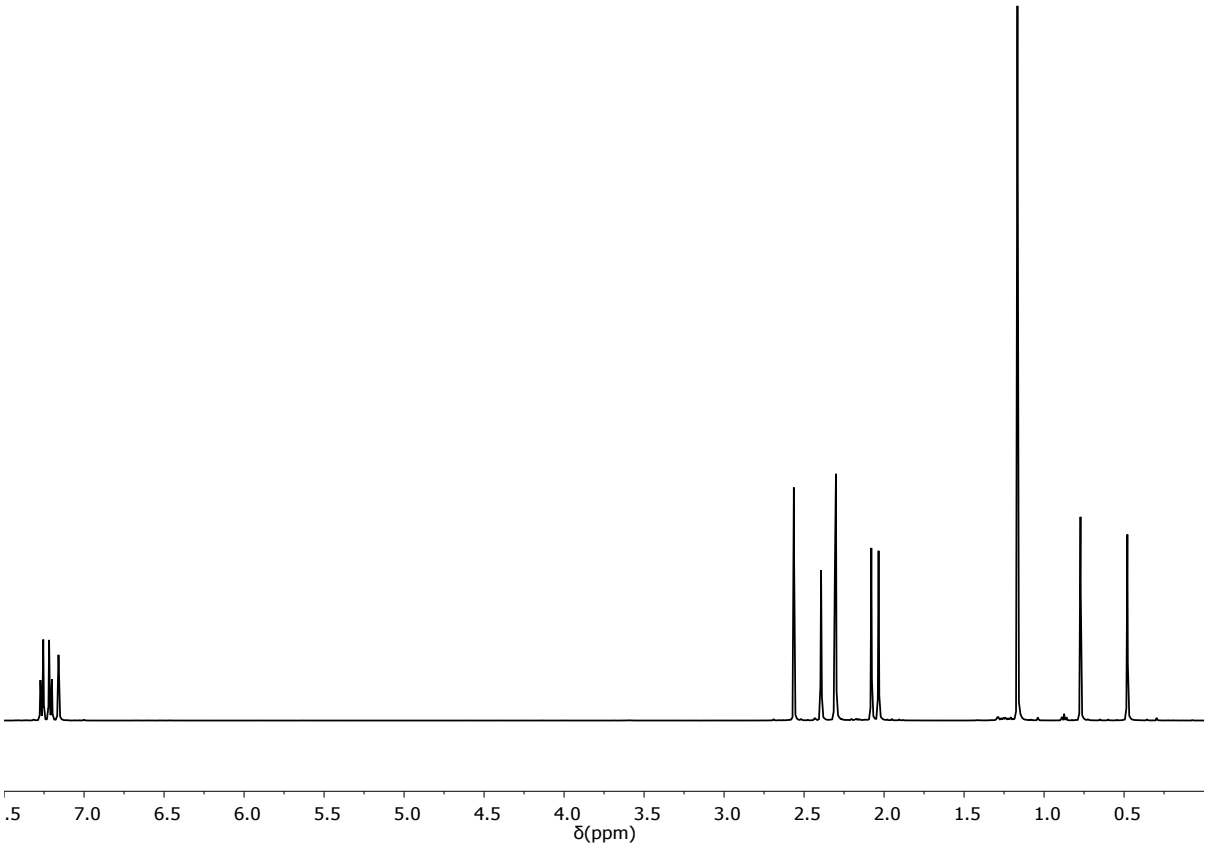


**Fig. S21** $^{1}$H NMR spectrum of $^{Me2}$SB($^{4\text{-}t\text{-}Bu\text{-}C_6H_4}$N,I*)$TiCl_2$ (499.9 MHz, $C_6D_6$, 298 K).

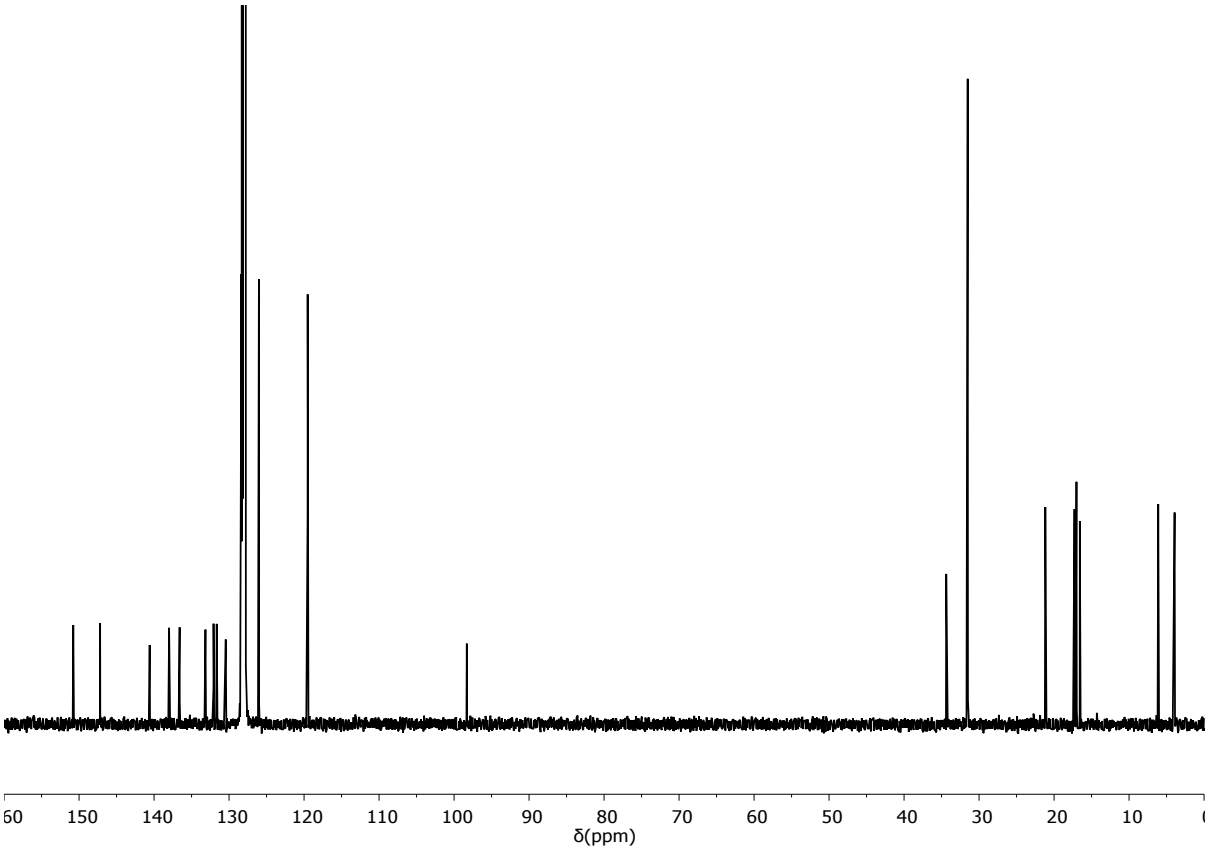


**Fig. S22** $^{13}$C{$^{1}$H} NMR spectrum of $^{Me2}$SB($^{4\text{-}t\text{-}Bu\text{-}C_6H_4}$N,I*)$TiCl_2$ (125.7 MHz, $C_6D_6$, 298 K).

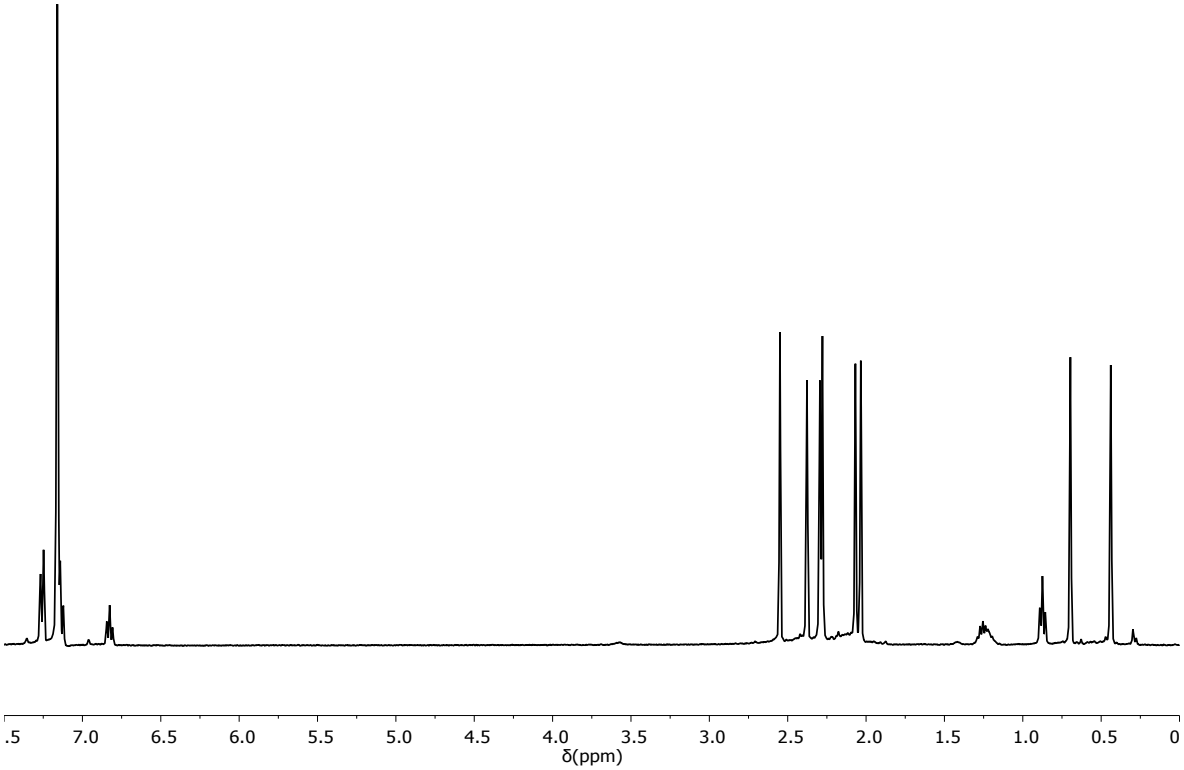


**Fig. S23** $^{1}$H NMR spectrum of $^{Me2}$SB($^{Ph}$N,I*)TiCl$_2$ (pentane: 0.87 and 1.23 ppm; 499.9 MHz, $C_6D_6$, 298 K).

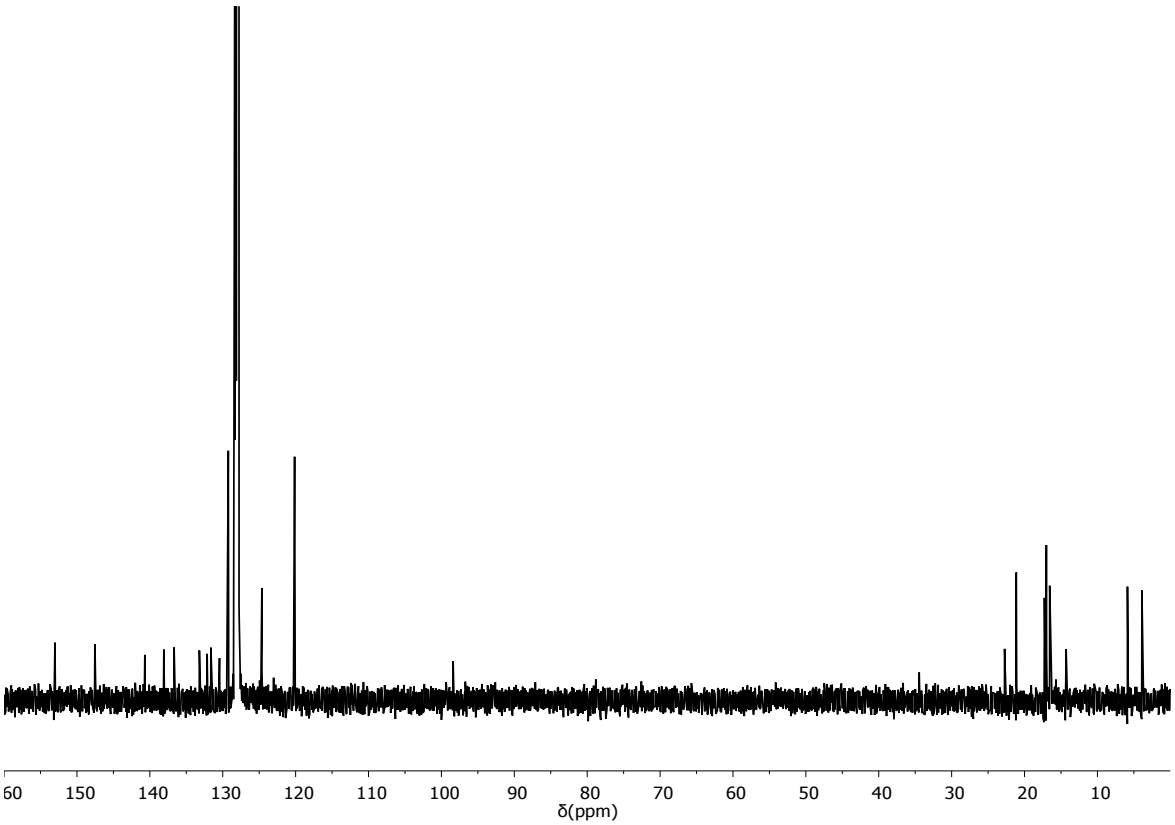


**Fig. S24** $^{13}$C{$^{1}$H} NMR spectrum of $^{Me2}$SB($^{Ph}$N,I*)TiCl$_2$ (125.7 MHz, $C_6D_6$, 298 K).

## 2.2 Support Procedure

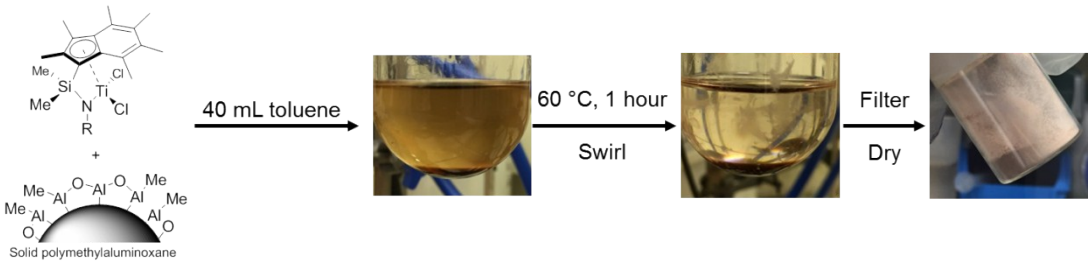


**Fig. S25** Pictorial representation of complex immobilisation for solid catalyst based on solid polymethylaluminoxane (sMAO) and $^{Me2}$SB($^{R}$N,I*)TiCl$_2$, sMAO-$^{Me2}$SB($^{R}$N,I*)TiCl$_2$.

**Table S1.** ICP-OES data of sMAO-$^{Me2}$SB($^{t\text{-}Bu}$N,I*)TiCl$_2$ and sMAO-$^{Me2}$SB($^{i\text{-}Pr}$N,I*)TiCl$_2$.

| **Complex** | **Time in slurry (h)** | **Weight % Al** | **Weight % Ti** | **Moles Al** | **Moles Ti** | **Al:Ti ratio** |
|---|---|---|---|---|---|---|
| $^{Me2}$SB($^{t\text{-}Bu}$N,I*)TiCl$_2$ | 0 | 26.2 | 0.24 | 0.971 | 0.005 | 194:1 |
| $^{Me2}$SB($^{i\text{-}Pr}$N,I*)TiCl$_2$ | 1 | 28.2 | 0.25 | 1.047 | 0.005 | 199:1 |
| $^{Me2}$SB($^{i\text{-}Pr}$N,I*)TiCl$_2$ | 2 | 28.6 | 0.24 | 1.061 | 0.005 | 208:1 |
| $^{Me2}$SB($^{i\text{-}Pr}$N,I*)TiCl$_2$ | 3 | 28.2 | 0.25 | 1.047 | 0.005 | 202:1 |

## 2.3 Solid state NMR spectoscopy

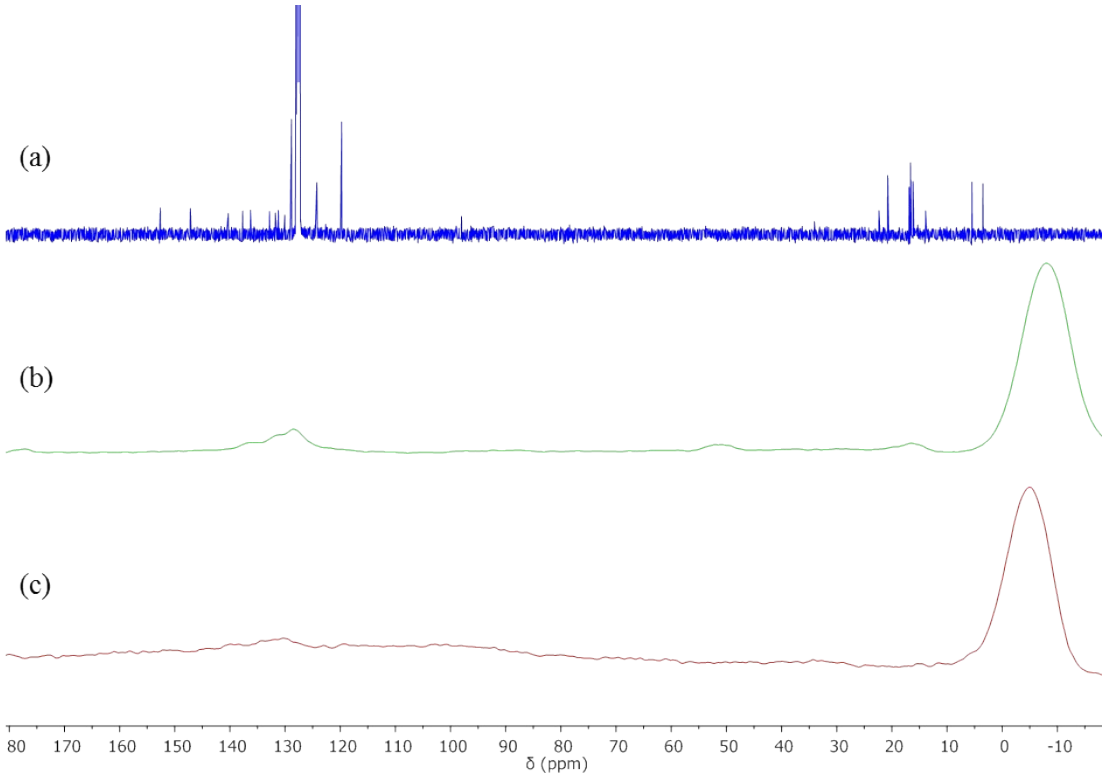


**Fig. S26** Stack plot of (a) $^{13}C\{^{1}H\}$ NMR spectrum of $^{Me2}SB(^{Ph}N,I^{*})TiCl_2$ (125.7 MHz, $C_6D_6$, 298 K), (b) $^{13}C$ CP-MAS (100.6 MHz) NMR spectrum of sMAO-$^{Me2}SB(^{Ph}N,I^{*})TiCl_2$ and (c) $^{13}C$ CP-MAS (100.6 MHz) NMR spectrum of sMAO.

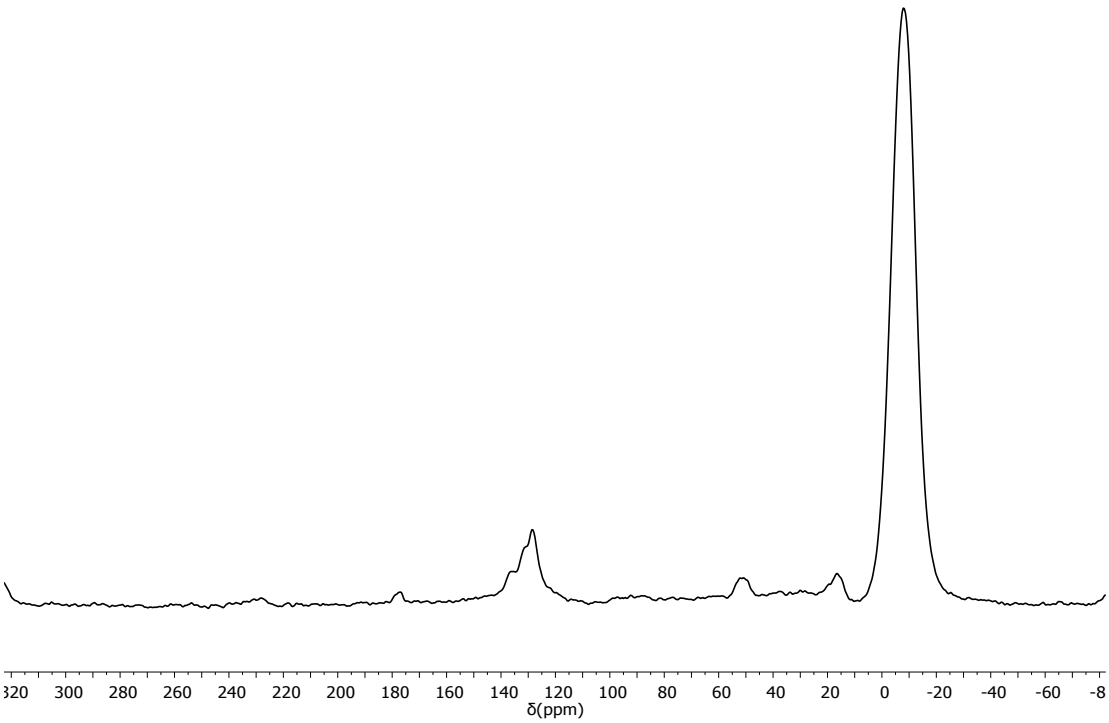


**Fig. S27** $^{13}C$ CP-MAS (100.6 MHz) NMR spectrum of sMAO-$^{Me2}SB(^{Ph}N,I^{*})TiCl_2$.

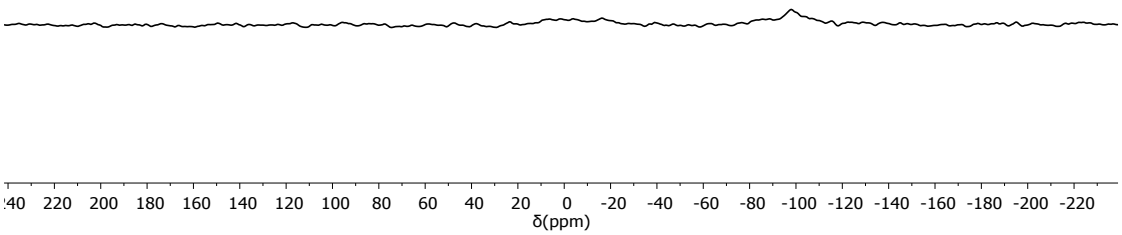


**Fig. S28** $^{29}$Si CP-MAS (79.4 MHz) NMR spectrum of sMAO-$^{Me2}$SB($^{Ph}$N,I*)$TiCl_2$.

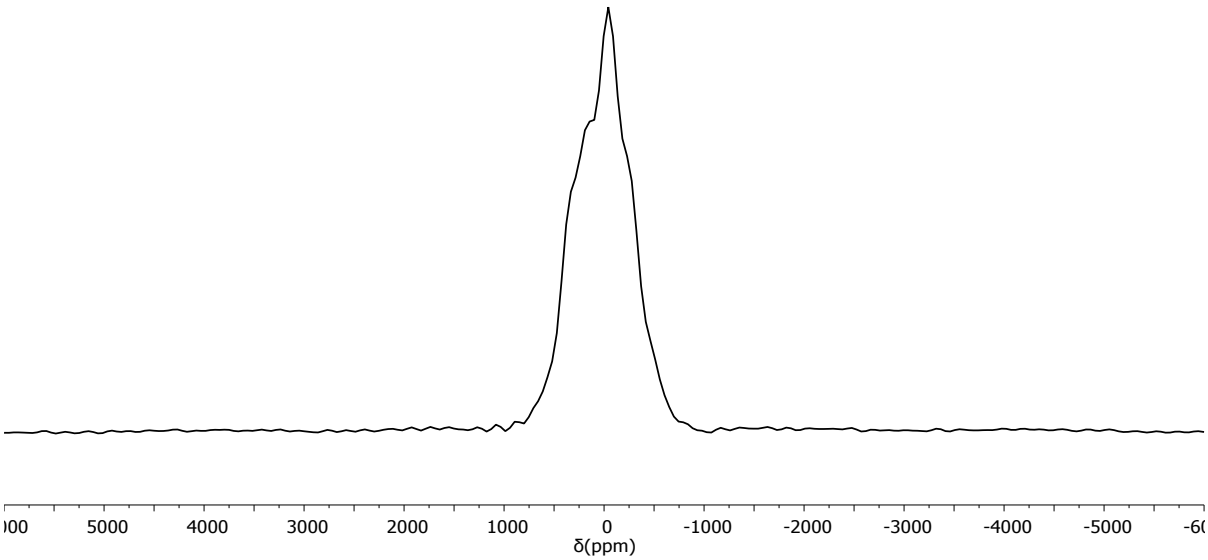


**Fig. S29** $^{27}$Al DP-MAS hahnecho (104.2 MHz) NMR spectrum of sMAO-$^{Me2}$SB($^{Ph}$N,I*)$TiCl_2$.

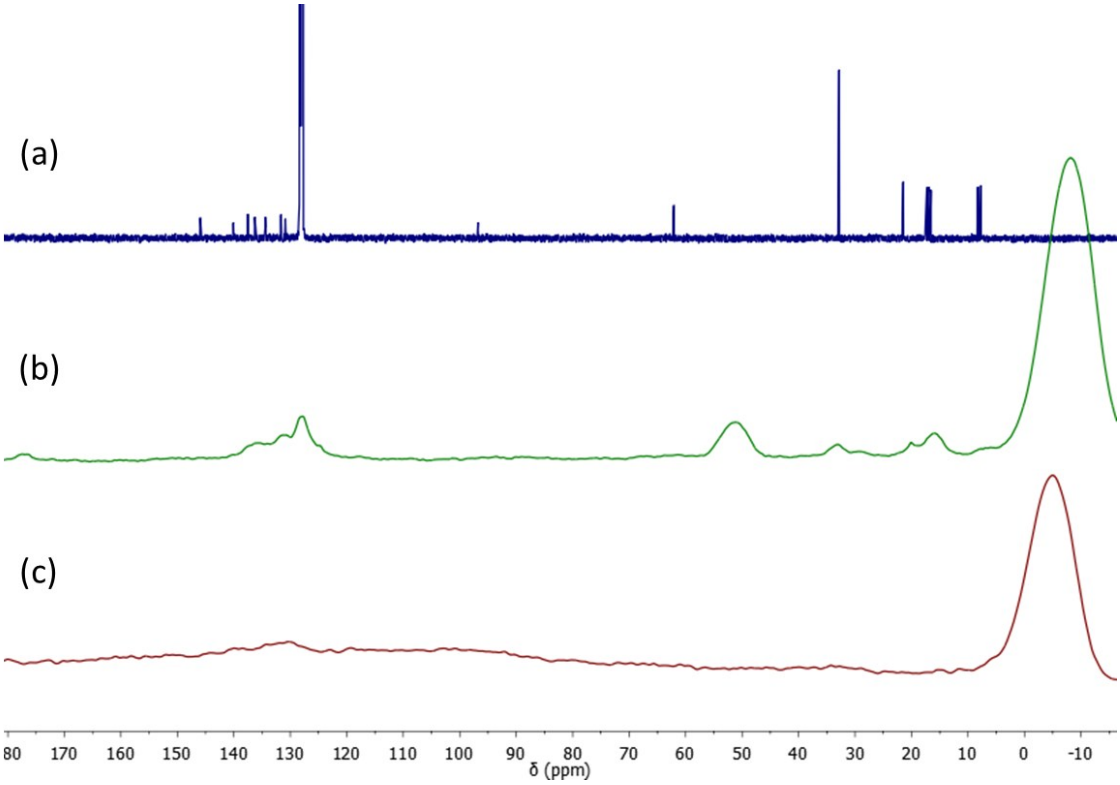


**Fig. S30** Stack plot of (a) $^{13}C\{^{1}H\}$ NMR spectrum of $^{Me2}SB(^{t\text{-}Bu}N,I^{*})TiCl_2$ (125.7 MHz, $C_6D_6$, 298 K), (b)$^{13}C$ CP-MAS (100.6 kHz) NMR spectrum of sMAO-$^{Me2}SB(^{t\text{-}Bu}N,I^{*})TiCl_2$ and (c) $^{13}C$ CP-MAS (100.6 kHz) NMR spectrum of sMAO.

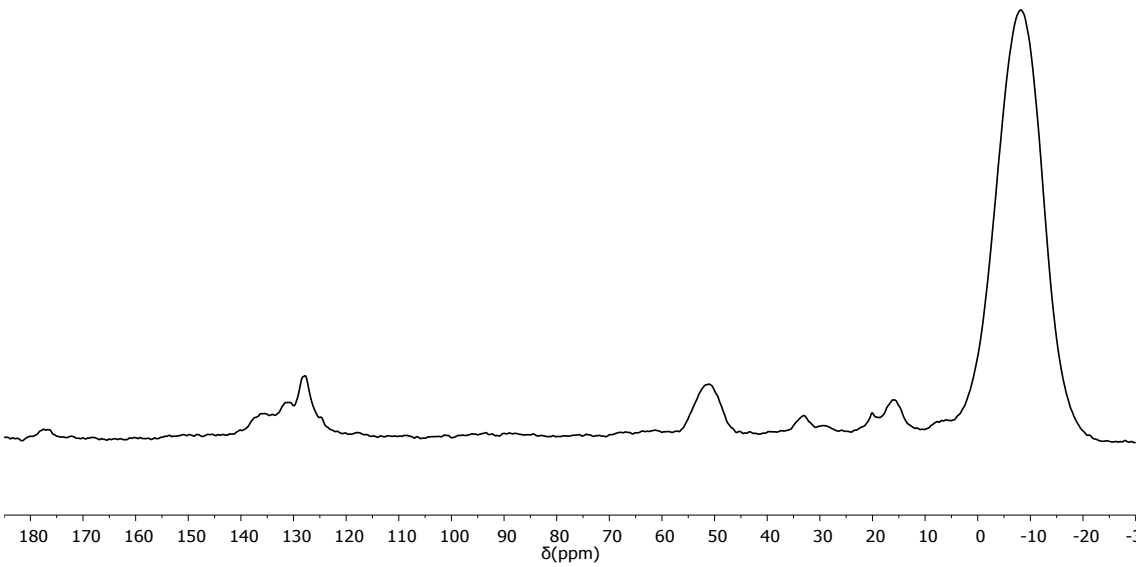


**Fig. S31** $^{13}C$ CP-MAS (100.6 kHz) NMR spectrum of sMAO-$^{Me2}SB(^{t\text{-}Bu}N,I^{*})TiCl_2$.

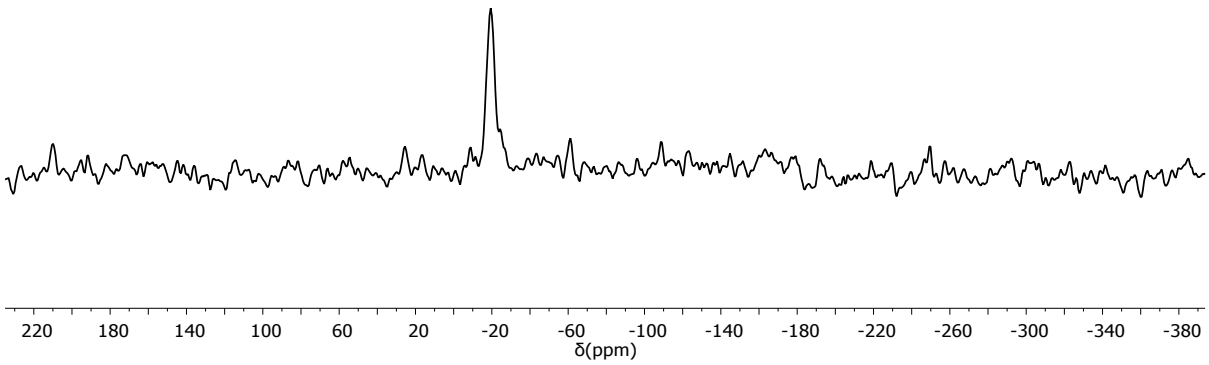


**Fig. S32** $^{29}$Si CP-MAS (79.4 MHz) NMR spectrum of sMAO-$^{Me2}$SB($^{t\text{-}Bu}$N,I*)$TiCl_2$.

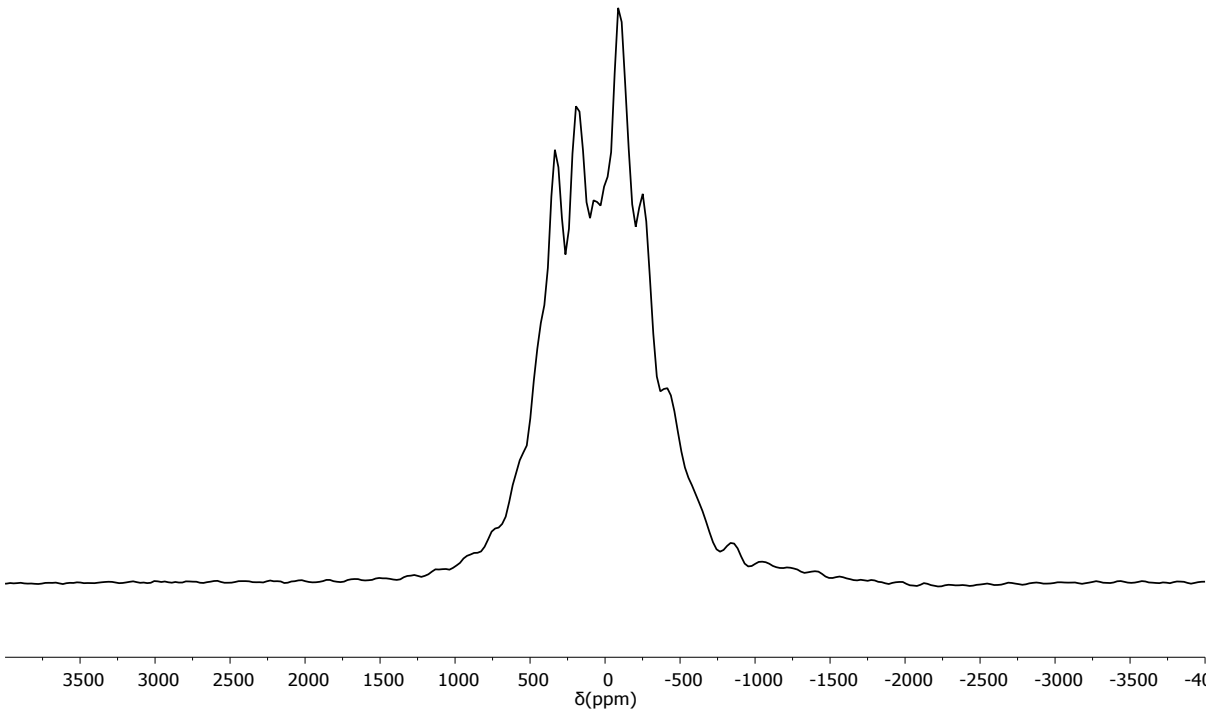


**Fig. S33** $^{27}$Al DP-MAS hahnecho (104.2 kHz) NMR spectrum of sMAO-$^{Me2}$SB($^{t\text{-}Bu}$N,I*)$TiCl_2$.

# 3 X-ray crystallography

**Table S2:** Selected experimental crystallographic data.

| Complex | $^{Me2}SB(^{t\text{-}Bu}N,I^*)TiCl_2$ | $^{Me2}SB(^{i\text{-}Pr}N,I^*)TiCl_2$ | $^{Me2}SB(^{4\text{-}t\text{-}Bu\text{-}C_6H_4}N,I^*)TiCl_2$ |
|---|---|---|---|
| **Crystal data** | | | |
| Chemical formula | $C_{21}H_{33}Cl_2NSiTi$ | $C_{20}H_{31}Cl_2NSiTi$ | $C_{27}H_{37}Cl_2NSiTi \cdot C_5H_{12}$ |
| $M_r$ | 446.37 | 432.35 | 594.61 |
| Crystal system, space group | Triclinic, $P\bar{1}$ | Monoclinic, $P2_1/c$ | Triclinic, $P\bar{1}$ |
| Temperature (K) | 150 | 150 | 150 |
| $a$, $b$, $c$ (Å) | 8.2680 (6), 11.8794 (7), 12.9943 (7) | 11.5225 (2), 12.9843 (2), 15.2891 (2) | 9.9660 (2), 12.4507 (4), 15.2615 (4) |
| $\alpha$, $\beta$, $\gamma$ (°) | 71.395 (5), 78.040 (5), 70.734 (6) | 90, 104.979 (2), 90 | 112.445 (3), 108.902 (2), 90.786 (2) |
| $V$ (Å$^3$) | 1134.41 (13) | 1839.60 (10) | 1635.29 (8) |
| $Z$ | 2 | 4 | 2 |
| Radiation type | Cu $K\alpha$ | Cu $K\alpha$ | Cu $K\alpha$ |
| μ (mm$^{-1}$) | 5.89 | 6.04 | 4.21 |
| Crystal size (mm) | 0.16 × 0.08 × 0.06 | 0.20 × 0.15 × 0.13 | 0.37 × 0.33 × 0.06 |
| **Data Collection** | | | |
| Diffractometer | SuperNova, Dual, Cu at zero, Atlas diffractometer | SuperNova, Dual, Cu at zero, Atlas diffractometer | SuperNova, Dual, Cu at zero, Atlas diffractometer |
| Absorption correction | Multi-scan *CrysAlis PRO* 1.171.38.41 (Rigaku Oxford Diffraction, 2015) Empirical absorption correction using spherical harmonics, implemented in SCALE3 | Multi-scan *CrysAlis PRO* 1.171.38.41 (Rigaku Oxford Diffraction, 2015) Empirical absorption correction using spherical harmonics, implemented in SCALE3 | Multi-scan *CrysAlis PRO* 1.171.38.41 (Rigaku Oxford Diffraction, 2015) Empirical absorption correction using spherical harmonics, implemented in SCALE3 |

| | | | |
|---|---|---|---|
| | ABSPACK scaling algorithm. | ABSPACK scaling algorithm. | ABSPACK scaling algorithm. |
| $T_{min}$, $T_{max}$ | 0.771, 1.000 | 0.578, 1.000 | 0.444, 1.000 |
| No. of measured, independent and observed [$I > 2\sigma(I)$] reflections | 9522, 4437, 3763 | 26674, 4617, 4178 | 18216, 6669, 6313 |
| $R_{int}$ | 0.030 | 0.032 | 0.035 |
| | | **Refinement** | |
| $R[F^2 > 2\sigma(F^2)]$, $wR(F^2)$, $S$ | 0.037, 0.129, 1.17 | 0.030, 0.094, 0.96 | 0.040, 0.119, 0.95 |
| No. of reflections | 4437 | 4617 | 6669 |
| No. of parameters | 246 | 235 | 395 |
| No. of restraints | 0 | 0 | 42 |
| $(\Delta/\sigma)_{max}$ | 0.001 | 0.001 | 0.001 |
| $\Delta\rho_{max}$, $\Delta\rho_{min}$ (e Å$^{-3}$) | 0.46, -0.45 | 0.38, -0.35 | 0.52, -0.28 |

Computer programs: *CrysAlis PRO* 1.171.38.41 (Rigaku OD, 2015), SUPERFLIP. Palatinus, L.; Chapuis, G. J. Appl. Cryst. 2007, 40, 786-790, Sir-92. Altomare, A.; Cascarano, G.; Giacovazzo, C.; Guagliardi, A. J. Appl. Cryst. 1994, 27, 435., *SHELXL2014* (Sheldrick, 2014), *ORTEP-3 for Windows*. Farrugia, L. J. J. Appl. Cryst. 1997, 30, 565.

# 4 Polymerisation study

## 4.1 Slurry phase polymerisation

**Table S3.** Slurry phase ethylene polymerisation using sMAO supported catalysts.

| Complex | T (°C) | Time (minutes) | Activity ± standard deviation ($kg_{PE}/mol_{Ti}/h/bar$) |
|---|---|---|---|
| sMAO-$^{Me2}$SB($^{t\text{-}Bu}$N,I*)$TiCl_2$ | 50 | 30 | 2958±215 |
| | 60 | 30 | 3602±132 |
| | 70 | 30 | 3524±275 |
| | 80 | 30 | 2981±164 |
| | 90 | 30 | 2565±38 |
| | 70 | 5 | 5562±363 |
| | 70 | 15 | 4580±158 |
| | 70 | 60 | 2973±138 |
| sMAO-$^{Me2}$SB($^{i\text{-}Pr}$N,I*)$TiCl_2$ | 50 | 30 | 1293±12 |
| | 60 | 30 | 1402±128 |
| | 70 | 30 | 1287±86 |
| | 80 | 30 | 1222±99 |
| | 90 | 30 | 976±49 |
| | 70 | 5 | 1916±381 |
| | 70 | 15 | 1521±75 |
| | 70 | 60 | 848±10 |
| sMAO-$^{Me2}$SB($^{n\text{-}Bu}$N,I*)$TiCl_2$ | 50 | 30 | 848±37 |
| | 60 | 30 | 666±15 |
| | 70 | 30 | 837±9 |
| | 80 | 30 | 814±66 |
| | 90 | 30 | 728±24 |
| | 70 | 5 | 2340±337 |
| | 70 | 15 | 1244±63 |
| | 70 | 60 | 360±32 |
| sMAO-$^{Me2}$SB($^{4\text{-}n\text{-}Bu\text{-}C_6H_4}$N,I*)$TiCl_2$ | 50 | 30 | 313±9 |
| | 60 | 30 | 357±9 |
| | 70 | 30 | 365±3 |
| | 80 | 30 | 409±11 |
| | 90 | 30 | 266±12 |
| | 70 | 5 | 666±67 |
| | 70 | 15 | 524±8 |
| | 70 | 60 | 259±15 |
| sMAO-$^{Me2}$SB($^{4\text{-}t\text{-}Bu\text{-}C_6H_4}$N,I*)$TiCl_2$ | 50 | 30 | 289±21 |
| | 60 | 30 | 323±20 |
| | 70 | 30 | 321±8 |
| | 80 | 30 | 308±64 |
| | 90 | 30 | 149±21 |
| | 70 | 5 | 632±32 |
| | 70 | 15 | 461±22 |
| | 70 | 60 | 255±4 |
| sMAO- $^{Me2}$SB($^{Ph}$N,I*)$TiCl_2$ | 50 | 30 | 300±6 |
| | 60 | 30 | 288±3 |
| | 70 | 30 | 263±20 |
| | 80 | 30 | 224±6 |

| | | | |
|---|---|---|---|
| sMAO- $^{Me2}$SB($^{Ph}$N,I*)TiCl$_2$ | 90 | 30 | 161±6 |
| | 70 | 5 | 441±25 |
| | 70 | 15 | 375±31 |
| | 70 | 60 | 235±11 |
| sMAO- $^{Me2}$SB($^{t\text{-}Bu}$N,Cp*)TiCl$_2$ | 50 | 30 | 979±96 |
| | 60 | 30 | 1308±25 |
| | 70 | 30 | 1289±17 |
| | 80 | 30 | 1105±71 |
| | 90 | 30 | 716±18 |
| sMAO-$^{Me2}$SB($^{t\text{-}Bu}$N,I*)TiCl$_2$ (Al:Ti = 100:1) | 50 | 30 | 895±36 |
| | 60 | 30 | 1033±61 |
| | 70 | 30 | 1160±35 |
| | 80 | 30 | 983±52 |
| | 90 | 30 | 735±50 |

## 4.2 Scanning electron microscopy

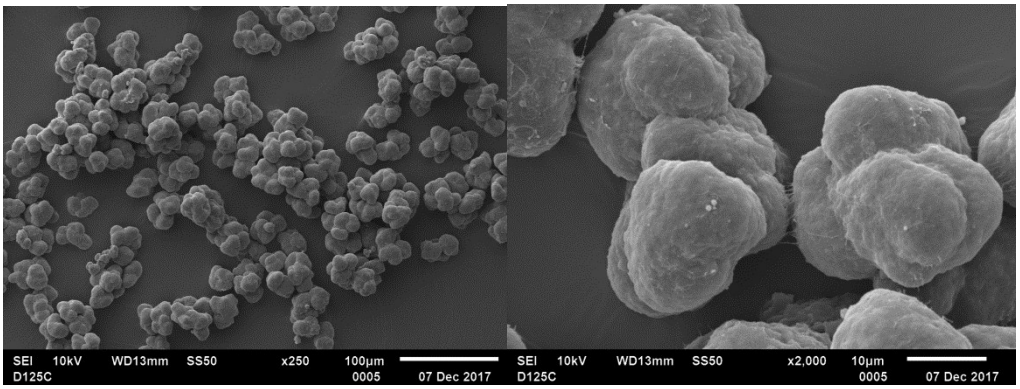


**Fig S34.** SEM images of polyethylene synthesised using sMAO-$^{Me2}$SB($^{t\text{-}Bu}$N,I*)TiCl$_2$. Polymerisation conditions: 2 bar ethylene, 50 mL hexanes, 10 mg pre-catalyst, 150 mg TIBA, 30 minutes, 70 °C.

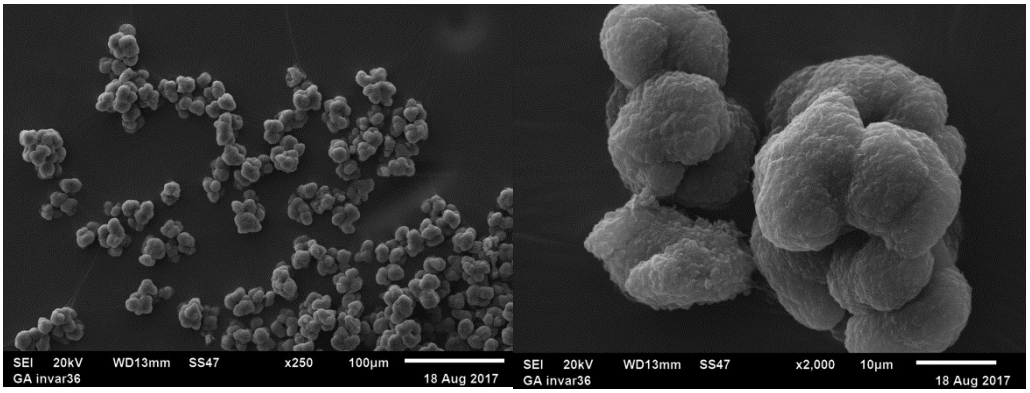


**Fig S35.** SEM images of polyethylene synthesised using sMAO-$^{Me2}$SB($^{i\text{-}Pr}$N,I*)TiCl$_2$. Polymerisation conditions: 2 bar ethylene, 50 mL hexanes, 10 mg pre-catalyst, 150 mg TIBA, 30 minutes, 70 °C.

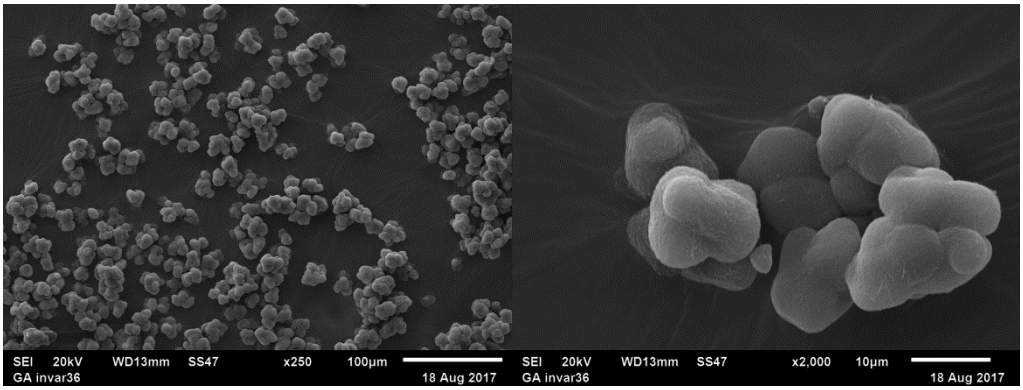


**Fig S36.** SEM images of polyethylene synthesised using sMAO-$^{Me2}$SB($^{n\text{-Bu}}$N,I*)TiCl$_2$. Polymerisation conditions: 2 bar ethylene, 50 mL hexanes, 10 mg pre-catalyst, 150 mg TIBA, 30 minutes, 70 °C.

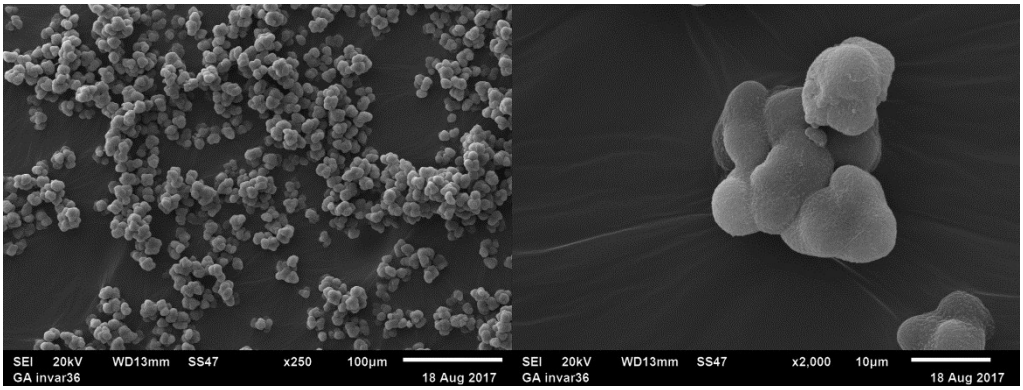


**Fig S37.** SEM images of polyethylene synthesised using sMAO- $^{Me2}$SB($^{4\text{-}n\text{-Bu-C}_6\text{H}_4}$N,I*)TiCl$_2$. Polymerisation conditions: 2 bar ethylene, 50 mL hexanes, 10 mg pre-catalyst, 150 mg TIBA, 30 minutes, 70 °C.

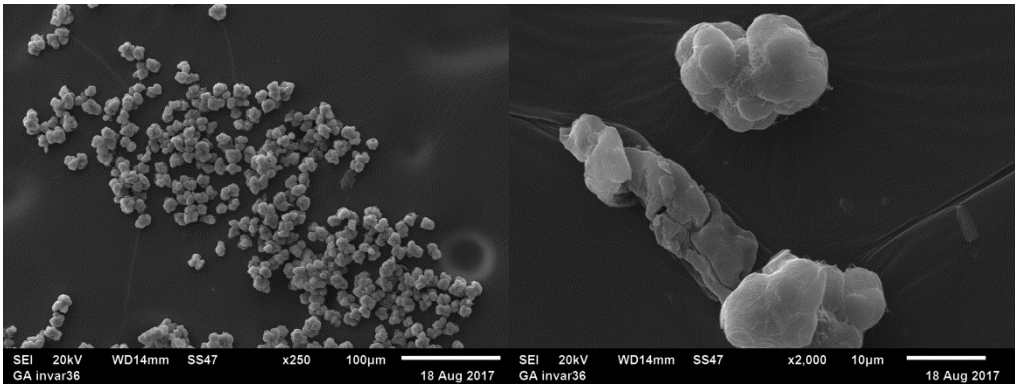


**Fig S38.** SEM images of polyethylene synthesised using sMAO-$^{Me2}$SB($^{4\text{-}t\text{-Bu-C}_6\text{H}_4}$N,I*)TiCl$_2$. Polymerisation conditions: 2 bar ethylene, 50 mL hexanes, 10 mg pre-catalyst, 150 mg TIBA, 30 minutes, 70 °C.

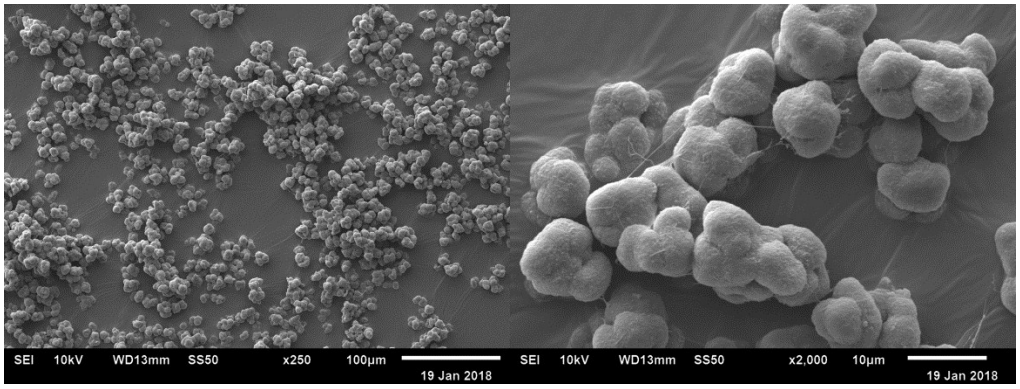


**Fig S39.** SEM images of polyethylene synthesised using sMAO-$^{Me2}$SB($^{Ph}$N,I*)$TiCl_2$. Polymerisation conditions: 2 bar ethylene, 50 mL hexanes, 10 mg pre-catalyst, 150 mg TIBA, 30 minutes, 70 °C.

# 5 References


1 D. F. Shriver, *The Manipulation of Air-Sensitive Compounds*, 2nd edn., 1986.

2 F. M. Alías, S. Barlow, J. S. Tudor, D. O'Hare, R. T. Perry, J. M. Nelson and I. Manners, *J. Organomet. Chem.*, 1997, **528**, 47–58.

3 J. P. Fackler, *Inorganic Syntheses*, John Wiley & Sons, Inc., Hoboken, NJ, USA, 1982, vol. 21.

4 J. Cosier and A. M. Glazer, *J. Appl. Crystallogr.*, 1986, **19**, 105–107.

5 CrysAlisPRO, Oxford Diffraction /Agilent Technologies UK Ltd, Yarnton, England.

6 Altomare, A.; Cascarano, G.; Giacovazzo, C.; Guagliardi, A.; Burla, M. C.; Polidori, G.; Camalli, M. *J. Appl. Crystallogr.* **1994**, *27*, 435.

7 L. Palatinus and G. Chapuis, J. Appl. Crystallogr., 2007, 40, 786-790.

8 L. J. Farrugia, J. Appl. Crystallogr., 1999, 32, 837-838.

9 A. L. Spek, J. Appl. Crystallogr., 2003, 36, 7-13.

10 L. J. Farrugia, J. Appl. Crystallogr., 1997, 30, 565.

11 L. Falivene, R. Credendino, A. Poater, A. Petta, L. Serra, R. Oliva, V. Scarano and L. Cavallo, *Organometallics*, 2016, **35**, 2286–2293.